

**IMPERIAL**

THE STUDY ON QUBIT-MOTION  
ENTANGLEMENT IN THE  
MØLMER-SØRENSEN GATE

Author

ZHI ZENG

CID: 06015879

Supervised by

DR YUE MA

10,112 words

A thesis submitted in partial fulfilment of the requirements for the degree of  
**Master of Science in Physics with Quantum Dynamics**

Department of Physics  
Imperial College London  
2025

# Abstract

Trapped ions are among the most promising platforms for practical quantum computing. However, as trapped-ion processors scale to larger sizes, their native entangling gate, the Mølmer–Sørensen (MS) gate, remains challenged by motional dissipation and imperfect calibration, where qubit-motion entanglement generated by the MS interaction plays a central role. Therefore, understanding the behavior of such qubit-motion entanglement is essential for addressing these noise. In this thesis, I theoretically investigate the role of qubit-motion entanglement in information flow, time miscalibration, and the emergence of non-completely positive (non-CP) reduced dynamics. Using the trace distance, I show that qubit-motion entanglement mediates bidirectional information flow in the coherent regime, while motional dissipation suppresses non-Markovian features and enforces effective Markovianity. By analyzing the propagator under time miscalibration, I reveal its decomposition into a noiseless MS gate and two error gates, and demonstrate that its quantum channel representation shares the same structure as motional dephasing. Finally, I construct a circuit of two time-miscalibrated MS gates, identifying constraints for non-CP behavior and showing that dissipation suppresses and eventually eliminates it. These findings clarify the structure of time miscalibration, elucidate the theoretical feasibility and fragility of exploiting residual entanglement as a resource for simulating non-Markovian dynamics, and provide groundwork for bridging theoretical models with experimental realizations in trapped-ion quantum platforms.

# **Declaration of Originality**

I hereby declare that the work presented in this thesis is my own unless otherwise stated. To the best of my knowledge the work is original and ideas developed in collaboration with others have been appropriately referenced.

## Acknowledgments

I would like to express my sincere gratitude to my supervisor, Dr. Yue Ma, for her patient guidance and valuable support throughout this project. Our discussions were often long and detailed, during which she provided careful and insightful advice that greatly shaped the direction of my research. Her feedback has been essential in improving the technical depth of this thesis. Beyond the project itself, her broader perspective has also influenced and refined my own physical taste.

# Contents

<b>Abstract</b>	i
<b>Declaration of Originality</b>	ii
<b>Acknowledgments</b>	iii
<b>1 Introduction</b>	1
<b>2 The Mølmer-Sørensen gate dynamics</b>	3
2.1 The ideal Mølmer-Sørensen gate . . . . .	3
2.1.1 The Mølmer-Sørensen Hamiltonian . . . . .	4
2.1.2 The Mølmer-Sørensen propagator . . . . .	5
2.2 The noisy Mølmer-Sørensen gate . . . . .	7
2.2.1 Categorization of errors in the Mølmer-Sørensen gate . . . . .	7
2.2.2 Dynamics under motional dissipation . . . . .	9
<b>3 Information flow through qubit-motion entanglement</b>	10
3.1 Trace distance and non-Markovianity . . . . .	11
3.2 Information flow in coherent dynamics . . . . .	12
3.3 Information flow in dissipative dynamics . . . . .	14
<b>4 Noise structure of time miscalibration</b>	19
4.1 Decomposition of MS propagator . . . . .	19
4.2 Error channel . . . . .	21
<b>5 Non-CP maps from time-miscalibrated MS gates</b>	24
5.1 Circuit model and the definition of the map . . . . .	25
5.2 The linearity of the effective map . . . . .	26
5.3 Constructing the effective map . . . . .	27
5.4 The region of the non-CP map in parameter space . . . . .	29
5.5 The effect of motional dissipation . . . . .	31
<b>6 Conclusions</b>	34
<b>References</b>	37

# 1

## Introduction

A major obstacle toward building practical quantum processors lies in the inherent fragility of their fundamental units—qubits. Unlike classical bits, qubits are highly susceptible to noise, including interactions with the environment and imperfect experimental control, leading to decoherence and unwanted coherent evolutions. Noise will lead to the loss of quantum information during processing, ultimately causing quantum computing (QC) to fail [1].

Currently, among various physical realizations, the trapped-ion quantum platform achieves the highest fidelities on quantum gate operations [2, 3]. In this platform, ions which are confined in radio-frequency Paul traps [4] and manipulated precisely using electromagnetic fields, serve as qubits, with carefully selected internal states representing  $|0\rangle$  and  $|1\rangle$ , while entanglement is achieved by using shared vibrational modes as a quantum bus. Although this type of platform provides high-fidelity operations, as systems scale towards large quantum processors, the impact of environmental noise and fluctuations in experimental parameters becomes increasingly significant. In particular, its native two-qubit entangling gate—the Mølmer-Sørensen (MS) gate—is a main source of error [5–10]. The main sources of noise in the MS gate are motional dissipation and imperfect experimental calibration [11–15], both of which are intrinsically linked to the qubit-motion entanglement generated by the MS interaction. Additionally, this very feature introduces a deviation between theory and experiment—when the experimental output state of an MS gate retains qubit-motion correlations, theorists typically trace out the motional degrees of freedom, thereby describing the qubit-motion system as a separable state. Accordingly, investigating how motional degrees of freedom govern the loss of quantum information from the qubits via qubit-motion entanglement, and exploring how MS-gate noise can be addressed through such entanglement, is not only crucial for understanding the physical foundations of trapped-ion QC, but also for advancing its practical utility, and may further help bridge the gap between theoretical models and experimental realizations.

To address noise in quantum processors, a range of strategies have been developed. For example, quantum error correction (QEC) aims to detect and correct errors through redundant qubits, enabling fault-tolerant QC in principle [16–20].

And quantum error mitigation (QEM) strives to reduce the impact of noise on computational results without requiring large-scale qubit overhead [21, 22]. However, in the current NISQ era, neither QEC nor QEM has proven completely practical. The former demands a large-scale qubit system and operations with fidelities exceeding the threshold required by certain correction codes, which is well beyond the capabilities of today’s quantum hardware. QEM methods, although more suited to NISQ devices, often rely on heavy post-processing or assumptions about the noise model, which can be inaccurate or hard to validate at scale. Rather than eliminating errors, another interesting strategy to deal with the quantum device noise is to exploit it. Instead of suppressing or correcting specific error channels, one can consider exploiting device noise to assist simulations of open quantum dynamics [23–25]. In this research paradigm, noise ceases to be purely detrimental and instead becomes a computational resource for simulating dissipative quantum dynamics.

Notably, the reduced qubit dynamics resulting from residual qubit-motion entanglement may naturally give rise to non-completely positive (non-CP) maps [26], and a sequence of such non-CP maps can constitute non-Markovian quantum processes [27, 28]. This observation motivates a natural idea: to exploit qubit-motion residual entanglement as a computational resource for simulating non-Markovian dynamics. To explore the feasibility of this idea, we focus on a representative noise that induces such residual entanglement, the time miscalibration.

This thesis theoretically investigates various aspects of qubit-motion entanglement in the MS gate, from its physical foundations to its potential utility in QC. Using QuTiP [29, 30], I numerically study the information flow of the qubit subsystem during MS evolution, characterizing non-Markovianity via the trace distance [31] both in the absence and presence of motional dissipation. In addition, I derive an analytical expression for the propagator of the MS gate under time miscalibration and, based on this propagator, construct non-CP maps by concatenating two time-miscalibrated MS gates. I further identify regions in parameter space where non-CP maps arise, and demonstrate that motional dissipation destroys such non-CP behavior. This study deepens the understanding of how motional degrees of freedom govern the loss of quantum information, and elucidate the theoretical feasibility of exploiting residual entanglement as a computational resource for simulating non-Markovian dynamics, thereby laying groundwork for future studies at the intersection of trapped-ion quantum computation and open quantum systems.

The remainder of the thesis is structured as follows:

- Chapter 2 introduces the theoretical foundations of the MS gate, including its Hamiltonian and propagator, the relevant noise sources and dissipative dynamics.
- Chapter 3 investigates the information flow within the qubit subsystem during MS evolution, introducing the concepts of trace distance and non-Markovianity, and examining both coherent and dissipative dynamics.
- Chapter 4 analyzes the propagator of time-miscalibrated MS gate and the error channel of time miscalibration.
- Chapter 5 demonstrates the construction of a non-CP map using two time-miscalibrated MS gates and analyzes the conditions for its existence.
- Chapter 6 summarizes the key findings and discusses directions for future research.

# 2

## The Mølmer-Sørensen gate dynamics

### Contents

---

<b>2.1</b>	<b>The ideal Mølmer-Sørensen gate</b>	<b>3</b>
2.1.1	The Mølmer-Sørensen Hamiltonian	4
2.1.2	The Mølmer-Sørensen propagator	5
<b>2.2</b>	<b>The noisy Mølmer-Sørensen gate</b>	<b>7</b>
2.2.1	Categorization of errors in the Mølmer-Sørensen gate	7
2.2.2	Dynamics under motional dissipation	9

---

### 2.1 The ideal Mølmer-Sørensen gate

In 1999, Mølmer and Sørensen introduced a quantum logic gate operating by generating a state-dependent force using bichromatic laser fields tuned near the first-order sideband transitions [5, 6]. Their scheme realizes a controlled-phase gate that does not require the ions to be prepared in the motional ground state since the internal and motional degrees of freedom are completely disentangled for all phonon number states  $n$ , marking a significant advancement over the earlier Cirac-Zoller gate [32]. An additional feature of the MS interaction is its ability to generate entanglement among multiple ions using only globally applied laser fields. Unlike gate schemes that require individual addressing of ions with tightly focused laser beams, the MS interaction simplifies experimental implementation while maintaining high-fidelity entanglement generation. Thus, the MS gate has since remained widely used in trapped-ion quantum computing.

### 2.1.1 The Mølmer-Sørensen Hamiltonian

Now, based on the first principle, I derive the MS Hamiltonian in the general field coupling regime. Consider two ions in a linear trap, the internal energy of an ion is described by the Hamiltonian (setting  $\hbar = 1$ )

$$H_0 = \nu a^\dagger a + \omega_0 \sigma_z / 2, \quad (2.1)$$

where  $\nu$  is the collective frequency,  $a^\dagger$  ( $a$ ) is the creation (annihilation) operator of the motional mode and  $\hbar\omega_0$  is the energy difference between the qubit states.

As shown in Fig. 2.1, each ion is addressed with two off-resonant laser pulses with frequency  $\omega_1 = \omega_0 + (\nu - \delta)$ ,  $\omega_2 = \omega_0 - (\nu - \delta)$  to mediate two-ion interactions, where  $\delta$  is the detuning to the first-order sideband.

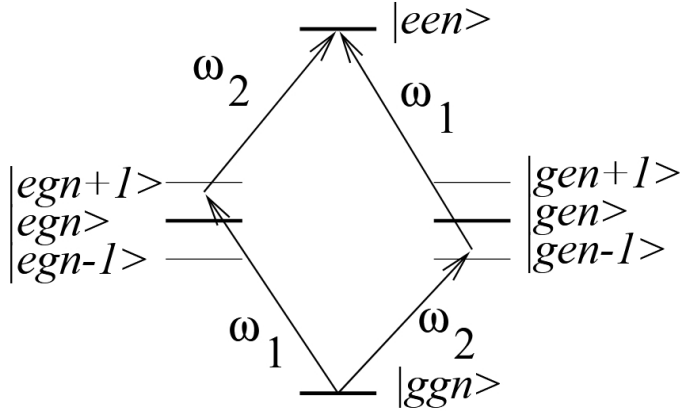


Figure 2.1: Schematic diagram for energy levels and laser drivings in MS interaction [5].

In the context of interaction between quantum particles and classical light, the electric field of the laser is

$$\begin{aligned} \vec{E}(x, t) &= \vec{E}_0 \cos(\omega_1 t - kx + \phi_1) + \vec{E}_0 \cos(\omega_2 t - kx + \phi_2) \\ &= 2\vec{E}_0 \cos[(\nu - \delta)t] \cos(\omega_0 t - kx + \phi), \end{aligned} \quad (2.2)$$

where we have set the laser phase  $\phi_1 = \phi_2 = \phi$ , which is experimentally realizable.

The interaction between ions and light is mainly the dipole transition. As the driving field is close to resonance with the transition between  $|g\rangle$  and  $|e\rangle$ , the effective dipole operator

$$\vec{d} = \sum_{i,j \in \{g,e\}} |i\rangle \langle i| \vec{d}|j\rangle \langle j| = \vec{d}_{ge}|g\rangle \langle e| + \vec{d}_{eg}|e\rangle \langle g| = \vec{d}_{eg}\sigma_x. \quad (2.3)$$

Under dipole approximation, the interaction Hamiltonian is given by

$$\begin{aligned} H_I &= -\vec{d} \cdot \vec{E} \\ &= 2\Omega \cos[(\nu - \delta)t] \sigma_x \otimes \cos(\omega_0 t - kx + \phi) \\ &= \Omega \cos[(\nu - \delta)t] [\sigma_+ e^{i\eta(a+a^\dagger)} e^{-i\omega_0 t} e^{-i\phi} + h.c.] / 2 \\ &= \Omega \cos[(\nu - \delta)t] [\sigma_+ (1 - i\eta(a+a^\dagger)) e^{-i\omega_0 t} e^{-i\phi} + h.c.] / 2, \end{aligned} \quad (2.4)$$

where the Rabi frequency  $\Omega \equiv -\vec{d}_{eg} \cdot \vec{E}_0$ ,  $\eta$  is the Lamb-Dicke parameter, and the third equality is obtained by applying the Lamb-Dicke approximation.

Transforming the interaction Hamiltonian into the interaction picture, and applying the rotating wave approximation (RWA) (when  $\delta \ll \nu$ ), we obtain

$$\begin{aligned}\tilde{H}_I &= \frac{\Omega}{4} [e^{i(\nu-\delta)t} + c.c.] [\sigma_+ (1 - i\eta(ae^{-i\nu t} + a^\dagger e^{i\nu t})) e^{-i\phi} + h.c.] \\ &= -i\eta \frac{\Omega}{4} \sigma_+ e^{-i\phi} (ae^{-i\delta t} + a^\dagger e^{i\delta t}) + h.c. \\ &= -i\eta \frac{\Omega}{4} (\sigma_+ e^{-i\phi} - \sigma_- e^{i\phi}) (ae^{-i\delta t} + a^\dagger e^{i\delta t}).\end{aligned}\quad (2.5)$$

Eq. (2.5) is the general MS Hamiltonian, which can be written in more common forms by appropriately selecting the laser phase  $\phi$ .

$$\tilde{H}_I = \begin{cases} (-1)^n \eta \Omega \sigma_y (ae^{-i\delta t} + a^\dagger e^{i\delta t}) / 2, & \text{if } \phi = n\pi, n \text{ is integer,} \\ (-1)^n \eta \Omega \sigma_x (ae^{-i\delta t} + a^\dagger e^{i\delta t}) / 2, & \text{if } \phi = n\pi - \pi/2. \end{cases} \quad (2.6)$$

Thus, the interaction Hamiltonian of a chain of  $N$  trapped ions is given by (just set  $\phi = \pi$ )

$$\tilde{H}_{\text{MS}} = -\eta \Omega (ae^{-i\delta t} + a^\dagger e^{i\delta t}) J_y, \quad (2.7)$$

where  $J_y = \sum_i^N \sigma_y^{(i)} / 2$  is the  $y$ -component of the collective spin operator.

### 2.1.2 The Mølmer-Sørensen propagator

For  $N$  ions MS Hamiltonian Eq. (2.7), it is a time-dependent Hamiltonian, so the propagator is

$$U(t, t_0) = T \exp \left[ -i \int_{t_0}^t H(t') dt' \right] \quad (2.8)$$

with  $T$  the time-ordering operator.

The equivalent practical forms for Eq. (2.8) are the Dyson series or the Magnus expansion [33]. Since  $[\tilde{H}_{\text{MS}}(t_1), [\tilde{H}_{\text{MS}}(t_2), \tilde{H}_{\text{MS}}(t_3)]] = 0$ , the terms after second order in the Magnus expansion form vanish. Hence, the Magnus expansion up to second order is an exact expression for Eq. (2.8), read as

$$U(t, 0) = \exp \left[ -i \int_0^t dt_1 \tilde{H}_{\text{MS}}(t_1) - \frac{1}{2} \int_0^t dt_1 \int_0^{t_1} dt_2 [\tilde{H}_{\text{MS}}(t_1), \tilde{H}_{\text{MS}}(t_2)] \right]. \quad (2.9)$$

To write the propagator the same as in Ref. [6], we should use Baker-Campbell-Hausdorff (BCH) formula and write Eq. (2.7) as

$$\tilde{H}_{\text{MS}} = f(t) J_y x + g(t) J_y p, \quad (2.10)$$

where we have introduced dimensionless position and momentum operators,  $x = \frac{1}{\sqrt{2}}(a + a^\dagger)$  and  $p = \frac{i}{\sqrt{2}}(a^\dagger - a)$ .

Define

$$\begin{aligned} F(t) &\equiv \int_0^t f(t')dt' \\ G(t) &\equiv \int_0^t g(t')dt' \\ A(t) &\equiv -\int_0^t F(t')g(t')dt', \end{aligned} \quad (2.11)$$

we can derive

$$U = e^{-iF(t)J_yx}e^{-iG(t)J_yp}e^{-iA(t)J_y^2} \quad (2.12)$$

with expressions

$$\begin{aligned} F(t) &= -\sqrt{2}\frac{\eta\Omega}{\delta}\sin(\delta t) \\ G(t) &= -\sqrt{2}\frac{\eta\Omega}{\delta}(1 - \cos(\delta t)) \\ A(t) &= -\frac{\eta^2\Omega^2}{\delta}(t - \frac{1}{2\delta}\sin(2\delta t)). \end{aligned} \quad (2.13)$$

Outside the weak field coupling regime, the qubit become strongly entangled with the motion during the gate operation. Following Ref. [6], for successful gate operation, it is necessary to guarantee that the motional degrees of freedom return to their initial state at the end of the gate. This requirement is satisfied by choosing parameters such that  $G(\tau) = F(\tau) = 0$ , corresponding to

$$\delta\tau = 2\pi K, \quad (2.14)$$

where  $K$  is an integer.

A maximally entangled state is generated when the parameters are further tuned to satisfy  $A(\tau) = -\pi/2$ . This condition can be realized by setting the ratio of coupling parameters according to

$$\frac{\eta\Omega}{\delta} = \frac{1}{2\sqrt{K}}. \quad (2.15)$$

By combing Eq. (2.14) and Eq. (2.15), we can express the time for gate duration as

$$\tau = \frac{\pi\sqrt{K}}{\eta\Omega}. \quad (2.16)$$

By choosing a small value of  $K$ , the gate can be performed faster.

Consider only a pair of trapped ions,  $J_y = (\sigma_y^{(1)} + \sigma_y^{(2)})/2$ , when the above requirements are met, we obtain the ideal MS gate

$$U_{\text{MS}} = \exp\left[i\frac{\pi}{4}\sigma_y^{(1)}\sigma_y^{(2)}\right]. \quad (2.17)$$

which can produce a maximally entangled state  $(|00\rangle - i|11\rangle)/\sqrt{2}$  from an initial product state  $|00\rangle$ .

Notably, Eq. (2.13) is independent of the motional quantum number  $n$ . As

a result, coherent evolution of the internal states is entirely decoupled from the motional state. Also,  $J_y$  in Eq. (2.13) is  $N$  ions collective spin operator, which means that it can generate entanglement among multiple ions using only globally applied laser fields.

## 2.2 The noisy Mølmer-Sørensen gate

The entangling gate constitutes the primary source of error in trapped-ion quantum information processing. Although the MS gate is intrinsically noise-resilient to initial motional state due to its ingenious design, its performance remains imperfect. Accordingly, in this section I present an overview of the error mechanisms associated with the MS gate, as well as methods for modeling its dynamics in the presence of noise. First, building on the first principle, I introduce a hierarchical categorization of MS-gate errors, structured into three levels: first-level, second-level, and third-level. Then, I discuss the calculation of MS dynamics under one of its dominant error sources—motional dissipation.

### 2.2.1 Categorization of errors in the Mølmer-Sørensen gate

By the physical nature, the gate errors can be broadly categorized into coherent and incoherent errors. Coherent errors are those manifest as systematic, deterministic deviations in the unitary evolution of the system, while incoherent errors arise from stochastic processes that cause irreversible loss of quantum information.

As shown in Fig. 2.2, coherent errors are classified into systematic errors and deterministic classical control errors. Systematic errors are inherent to the system due to imperfect modeling or unwanted couplings, and they can be explicitly subdivided into theoretical approximation errors and crosstalk.

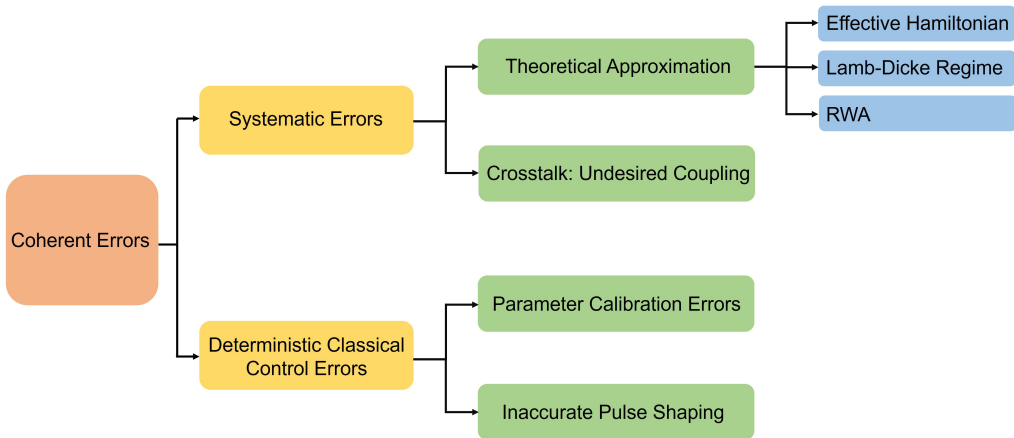


Figure 2.2: A hierarchical tree of coherent errors.

In the context of MS gate, the common analytical approximation errors arise from four sources: the effective Hamiltonian approximation, the Lamb-Dicke approximation (where the Lamb-Dicke parameter  $\eta \ll 1$ ), and RWA. When the gate speed becomes too fast, off-resonant terms contribute non-negligibly, causing the

RWA to break down, which in turn limits the achievable gate speed. Moreover, in some cases the system operates beyond the Lamb-Dicke regime—particularly when strong ion-motion interactions or higher motional states are involved [34].

Crosstalk between ions [9, 35], mainly the undesired coupling between qubits and non-targeted motional modes, will amplify noise sensitivity. It often becomes significant in many-ion systems with a complex multi-mode structure. This arises because the coupling strengths corresponding to different vibrational modes become comparable in magnitude and vary across different ions in the chain. In such systems, selectively driving a single mode unavoidably triggers higher-order phonon exchange processes, inadvertently coupling non-targeted spectator modes to the qubit states.

As for deterministic classical control errors, they often consist of inaccurate pulse shaping leading to phase and amplitude errors, and parameter calibration errors including fixed miscalibration of pulse durations and detunings.

Thus, coherent errors are typically systematic and, in many cases, can be corrected with proper calibration or optimized pulse design.

Similarly, as shown in Fig. 2.3, within the first-level classification of incoherent errors, decoherence effects and stochastic classical control errors are further categorized at the second level. This kind of errors arise from the environment or stochastic control fluctuations, often setting a fundamental limit on gate fidelity.

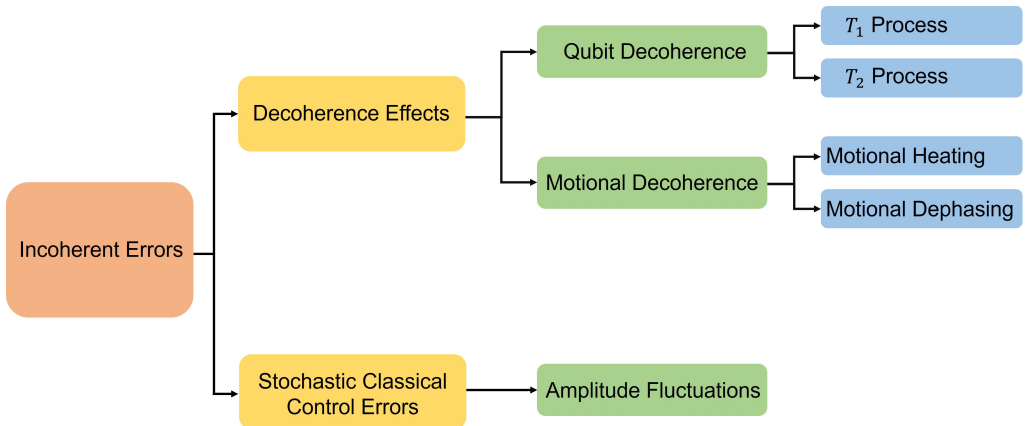


Figure 2.3: A hierarchical tree of incoherent errors.

The discussion of decoherence errors can be categorized into two distinct aspects: decoherence of the qubit state and decoherence of the motional state.

The qubit decoherence is characterized by two fundamental timescales:  $T_1$ , the energy relaxation time, and  $T_2$ , the phase coherence time. Energy relaxation results from coupling between the qubit and its environment, leading to population decay between the ground and excited states. For optical qubits, spontaneous photon emission and thermalization contribute to energy loss, whereas for hyperfine qubits,  $T_1$  is effectively infinite on typical gate timescales due to the absence of spontaneous decay. Phase decoherence arises from fluctuations in the relative phase between the qubit's basis states due to environmental noise. The dominant physical sources include magnetic field fluctuations and laser phase noise. Basically, the decoherence of the qubit state for trapped ion platform is negligible due to its sufficient long internal-state coherence time.

In contrast, the decoherence of motional mode can severely impact the overall gate performance [11]. This decoherence arises from two primary mechanisms: motional heating and motional dephasing. Motional heating occurs when the ion's motional state absorbs energy from environmental noise, leading to an increase in the average phonon number. The dominant sources include fluctuations in the trapping potential, ambient stray electric fields, and imperfections in the trap electrodes or power supplies. Motional dephasing is the loss of phase coherence in the motional state caused by variations in the radio-frequency drive, slow drifts or noise in control voltages, and mechanical vibrations or acoustic noise.

Stochastic classical control errors come from fluctuations in control parameters, mainly the amplitude instabilities [36]. These errors manifest as fluctuations in the intensity of control fields.

### 2.2.2 Dynamics under motional dissipation

Typically, noise refers to errors beyond those arising from theoretical approximations. Here, we focus on the dominant source of dissipation in MS evolution—motional dissipation [11–13]. Analogous to how the Schrödinger equation governs the unitary dynamics of a closed quantum system, the general framework for describing the dynamics of an open quantum system is provided by the Lindblad master equation, characterized by the generator[37]

$$\mathcal{L}[\circ] = -i[H(t), \circ] + \sum_{j=+,-,d} \gamma_j \mathcal{D}_{E_j}[\circ]. \quad (2.18)$$

The first term, describing unitary evolution, corresponds to the Liouville–von Neumann equation, which is the density-matrix generalization of the Schrödinger equation. The second term is the dissipator, defined as

$$\mathcal{D}_{\hat{O}}[\circ] = \hat{O} \circ \hat{O}^\dagger - \frac{1}{2} \{ \hat{O}^\dagger \hat{O}, \circ \}, \quad (2.19)$$

with Lindblad operators  $E_+ = a^\dagger$  and  $E_- = a$  for motional heating, and  $E_d = a^\dagger a = \hat{n}$  for motional dephasing.

In all subsequent sections involving motional dissipation, Eq. (2.18) serves as the basis for numerical simulations.

The Lindblad master equation provides a rigorous framework for describing the full process of the dissipative MS gate. Alternatively, the noisy implementation of the MS gate can be modeled by applying an appropriate quantum channel, corresponding to a specific noise mechanism, after the noiseless MS gate. For instance, in the case of motional dephasing, the noisy MS gate can be expressed as an ideal MS gate concatenated with a dephasing channel, whose canonical Kraus operators take the form [25]

$$\begin{aligned} K_1 &= a_1 I + a_3 J_y^2, \\ K_2 &= k_2 J_y, \\ K_3 &= a_2 I + a_4 J_y^2, \end{aligned} \quad (2.20)$$

where the coefficients are determined by the dephasing rate and system parameters.

# 3

## Information flow through qubit-motion entanglement

### Contents

---

3.1 Trace distance and non-Markovianity . . . . .	11
3.2 Information flow in coherent dynamics . . . . .	12
3.3 Information flow in dissipative dynamics . . . . .	14

---

The formation of correlations in a bipartite quantum system is intrinsically linked to the exchange of information between its subsystems. Consider the case where the bipartite system consists of an open quantum system and its environment, such correlations can be understood as the mechanism by which information about the system is partially lost to, or in some cases recovered from, the environment.

A simple way to illustrate this idea is to consider a simple open quantum system initially uncorrelated with its environment,

$$|\Psi(0)\rangle = \sum_i \Psi_i |i\rangle \otimes |\Phi\rangle, \quad (3.1)$$

and evolving under a joint system-environment unitary operator

$$U = \sum_i |i\rangle\langle i| \otimes u_i(t). \quad (3.2)$$

At time  $t$ , the state becomes

$$|\Psi(t)\rangle = \sum_i \Psi_i |i\rangle \otimes u_i(t) |\Phi\rangle \quad (3.3)$$

in which the system and environment are no longer independent, i.e., correlations in the form of system-environment entanglement have been generated. Consequently,

the environment acquires partial information about the system.

Analogously, in the case of Mølmer-Sørensen (MS) dynamics, the bipartite system consists of the qubits subsystem and the motional mode. The entanglement generated between them thus naturally corresponds to an exchange of information, whereby the qubits imprint part of their state onto the motion, and the motional state in turn can influence the subsequent qubit dynamics. The aim of this chapter is to characterize the information flow of the qubit subsystem induced by the qubit-motion entanglement and to identify whether the qubit dynamics is non-Markovian.

Thus, we require a quantitative tool that connects information flow with observable properties of the reduced qubit dynamics. One particularly useful quantity in this regard is the trace distance [31], which provides a measure of how distinguishable two quantum states are. Since the distinguishability of states directly reflects how much information about the system remains accessible, the time dependence of the trace distance naturally encodes the direction of information flow. This observation leads to a clear operational criterion for non-Markovianity—Markovian processes are characterized by a monotonic decrease of the trace distance between any two initial states, while non-Markovian dynamics are signaled by time intervals where the trace distance increases, corresponding to a partial backflow of information from the environment to the system [27].

In the following, I first introduce the trace distance in detail and its role in characterizing non-Markovian dynamics (Sec. 1). I then apply this framework to analyze numerical simulations of MS evolution in both ideal and dissipative cases (Secs. 2 and 3).

### 3.1 Trace distance and non-Markovianity

In open quantum dynamics, the information flow between the system and its environment is often associated with the correlations that allow the environment to acquire partial information about the system. From the perspective of the reduced system alone, such a flow manifests itself as a reduction in our ability to distinguish different initial states based solely on the system’s subsequent evolution [27].

A natural way to quantify this distinguishability is through the trace distance, defined as

$$D(\rho_1, \rho_2) = \frac{1}{2} \text{Tr} |\rho_1 - \rho_2|, \quad (3.4)$$

where  $|A| = \sqrt{A^\dagger A}$ . The trace distance  $D$  represents a metric on the space of density matrices, bounded as  $0 \leq D \leq 1$ . It quantifies the distinguishability between the two quantum states  $\rho_1$  and  $\rho_2$ .

The basic idea underlying the connection with Markovianity can be stated as follows. In Markovian processes, the distinguishability between any two initial states decreases monotonically over time. By contrast, non-Markovian processes are characterized by intervals where distinguishability temporarily increases.

Interpreting the loss of distinguishability as a flow of information from the open system to its environment, one is thus led to an intuitive picture—the key signature of non-Markovian dynamics is a reversed flow of information, i.e., a partial return of information from the environment back to the open system.

To formalize this, we consider the rate of change of the trace distance defined by

$$\sigma(t, \rho_{1,2}(0)) = \frac{d}{dt} D(\rho_1(t), \rho_2(t)). \quad (3.5)$$

which depends on both time  $t$  and the chosen pair of initial states  $\rho_{1,2}(0)$  for a given quantum process. A process is said to be non-Markovian if there exist initial states and a time  $t$  such that

$$\sigma(t, \rho_{1,2}(0)) > 0, \quad (3.6)$$

or equivalently

$$D(\rho_1(t + dt), \rho_2(t + dt)) > D(\rho_1(t), \rho_2(t)). \quad (3.7)$$

Any observed growth of the trace distance therefore serves as a direct and representation-independent signature of non-Markovianity. Importantly, this criterion does not rely on the existence of a master equation or on any specific approximations [27], making it particularly suitable for analyzing the MS evolution, where the interplay between qubit and motional degrees of freedom naturally gives rise to complex correlation dynamics.

## 3.2 Information flow in coherent dynamics

I began by studying the time dependence of the trace distance  $D(\rho_1, \rho_2; t)$  of different pairs of initial qubit states during a single MS gate, in the absence of any dissipation. In this case, the dynamics of the combined qubit-motion system is purely unitary, so that no information is irretrievably lost to the environment. Equivalently, the total system conserves information.

In the analysis, two coupling regimes are considered—a weak field coupling regime and a general field coupling regime. For each regime, I compare four representative initial states of the qubits: the product states  $|00\rangle\langle 00|$  and  $|11\rangle\langle 11|$ , as well as two maximally entangled Bell states  $|\Phi^+\rangle\langle\Phi^+|$  and  $|\Psi^-\rangle\langle\Psi^-|$  with

$$|\Phi^+\rangle = \frac{1}{\sqrt{2}}(|00\rangle + |11\rangle), \quad (3.8)$$

$$|\Psi^-\rangle = \frac{1}{\sqrt{2}}(|01\rangle - |10\rangle). \quad (3.9)$$

These choices allow us to contrast separable and entangled cases within a unified framework. The corresponding results are shown in Fig. 3.1, while the detailed parameters of each coupling regime are specified in the caption.

In Fig. 3.1, the trace distance  $D$  exhibits a pronounced periodic oscillatory behavior. Each full oscillation period is naturally associated with a closed trajectory of the motional state in phase space. Within each period,  $D$  first decreases and then increases, indicating that information initially flows from the qubits into the motion, thereby reducing the distinguishability of the qubit states, and at later times within the same cycle, the motion feeds information back into the qubits, causing  $D$  to rise again. This recovery of distinguishability provides a clear signature of

non-Markovian dynamics in the reduced qubit evolution.

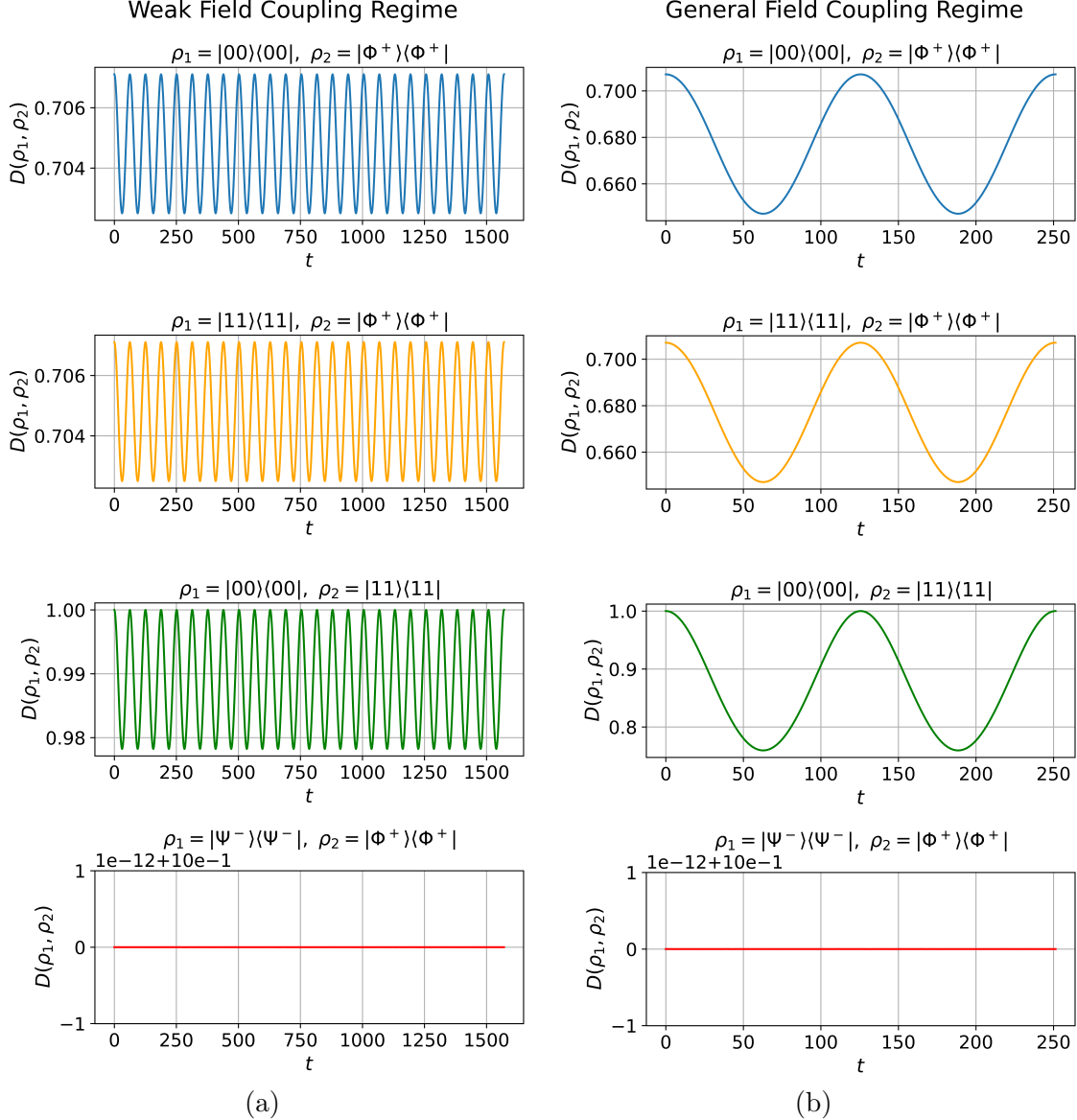


Figure 3.1: Plots of the trace distance  $D$  as a function of time  $t$  for different pairs of initial two-qubit states during a single MS gate. (a) Weak field coupling regime with parameters  $\eta = 0.1$ ,  $\delta = 0.1\nu$ ,  $\Omega = 0.1\nu$ . (b) General field coupling regime with parameters  $\eta = 0.1$ ,  $\delta = 0.05\nu$ ,  $\Omega = 0.177\nu$ .

Next I compare different field coupling regimes for the same pair of initial qubit states. The parameter choices for the weak and general field regimes follow Ref. [6]. In the weak field regime, the condition  $\eta\Omega \ll \delta$  holds, implying a relatively small Rabi frequency  $\Omega$  and a larger detuning  $\delta$ .

As shown in Fig. 3.1, the duration of a single round in the weak field regime is half of that in the general field regime. This arises because in the weak field case the detuning  $\delta$  is twice as large, and according to Eq. (11), the time required to complete one loop in phase space scales inversely with  $\delta$ . Furthermore, from Eq. (12), the minimal gate time corresponds to 25 rounds in the weak field regime,

compared to only 2 rounds in the general regime. Consequently, Fig. 3.1(a) displays 25 oscillation cycles, whereas Fig. 3.1(b) shows only 2. In addition, the amplitude of oscillations in  $D$  is larger in the general coupling regime. This can be traced to the entanglement term in the evolution operator, which is proportional to  $\eta\Omega/\delta$ , leading to stronger qubit-motion entanglement and thereby increasing the depth of information exchange. In other words, stronger coupling not only accelerates the dynamics but also enhances the extent of non-Markovian information backflow.

In order to further clarify the role of the initial qubit states, I compare the time dependence of the trace distance within the same coupling regime but for different state pairs, taking Fig. 3.1(b) as an example. Since  $\langle \Phi^+ | 00 \rangle = \langle \Phi^+ | 11 \rangle = 1/\sqrt{2}$ , while  $|00\rangle$  and  $|11\rangle$  are mutually orthogonal, and likewise  $|\Phi^+\rangle$  and  $|\Psi^-\rangle$  are orthogonal, their corresponding initial trace distances are nonzero and unity, respectively.

Interestingly, although both the separable pair ( $|00\rangle, |11\rangle$ ) and the entangled pair ( $|\Phi^+\rangle, |\Psi^-\rangle$ ) are orthogonal, their subsequent behaviors differ markedly. For separable states, once correlations with the motional mode are established, the reduced qubit states are no longer orthogonal, so the trace distance falls below unity and exhibits oscillatory variations. By contrast, the two Bell states  $|\Phi^+\rangle$  and  $|\Psi^-\rangle$  represent the invariant states of the MS Hamiltonian. So the orthogonality of the two Bell states is preserved throughout the evolution, and the trace distance remains fixed at  $D = 1$ , unaffected by the information flow between qubits and motion.

This contrast highlights a subtlety: certain pairs of initial states may be insensitive to the signatures of non-Markovianity, as their mutual distinguishability does not encode the information exchange. Therefore, in order to reliably diagnose non-Markovian effects, it is necessary to test a sufficiently large sample of initial state pairs. Analogous observations hold in the weak field coupling regime.

In this section, I employed the trace distance as a reliable observable to visualize the information flow induced by qubit-motion entanglement during MS evolution. The results demonstrate that the reduced qubit dynamics is inherently non-Markovian. Moreover, stronger coupling not only accelerates the dynamics but also enhances the strength of non-Markovian information backflow. Finally, the analysis shows that testing a sufficiently large set of initial state pairs is essential for a faithful characterization of non-Markovian effects.

### 3.3 Information flow in dissipative dynamics

To investigate the impact of environmental noise on the information flow, we fix both the coupling regime and the choice of initial states, and then introduce motional dissipation. In the following analysis, we consider the weak field coupling regime with the same parameters as in Fig. 3.1(a), and select the pair ( $|00\rangle, |11\rangle$ ) as the initial qubit states. Dissipative effects from motional dephasing and heating are described by the collapse operators [6, 11]

$$C_1 = \sqrt{\gamma (1 + n_{th})} a, \quad C_2 = \sqrt{\gamma n_{th}} a^\dagger \quad C_3 = \sqrt{\gamma_P} a^\dagger a \quad (3.10)$$

where  $\gamma_P$  denotes the dephasing rate,  $\gamma$  the heating rate, and  $n_{\text{th}}$  the mean thermal phonon number.

Figure 3.2 shows the time dependence of the trace distance  $D$  and its derivative  $\sigma$  for the case of pure motional dephasing.

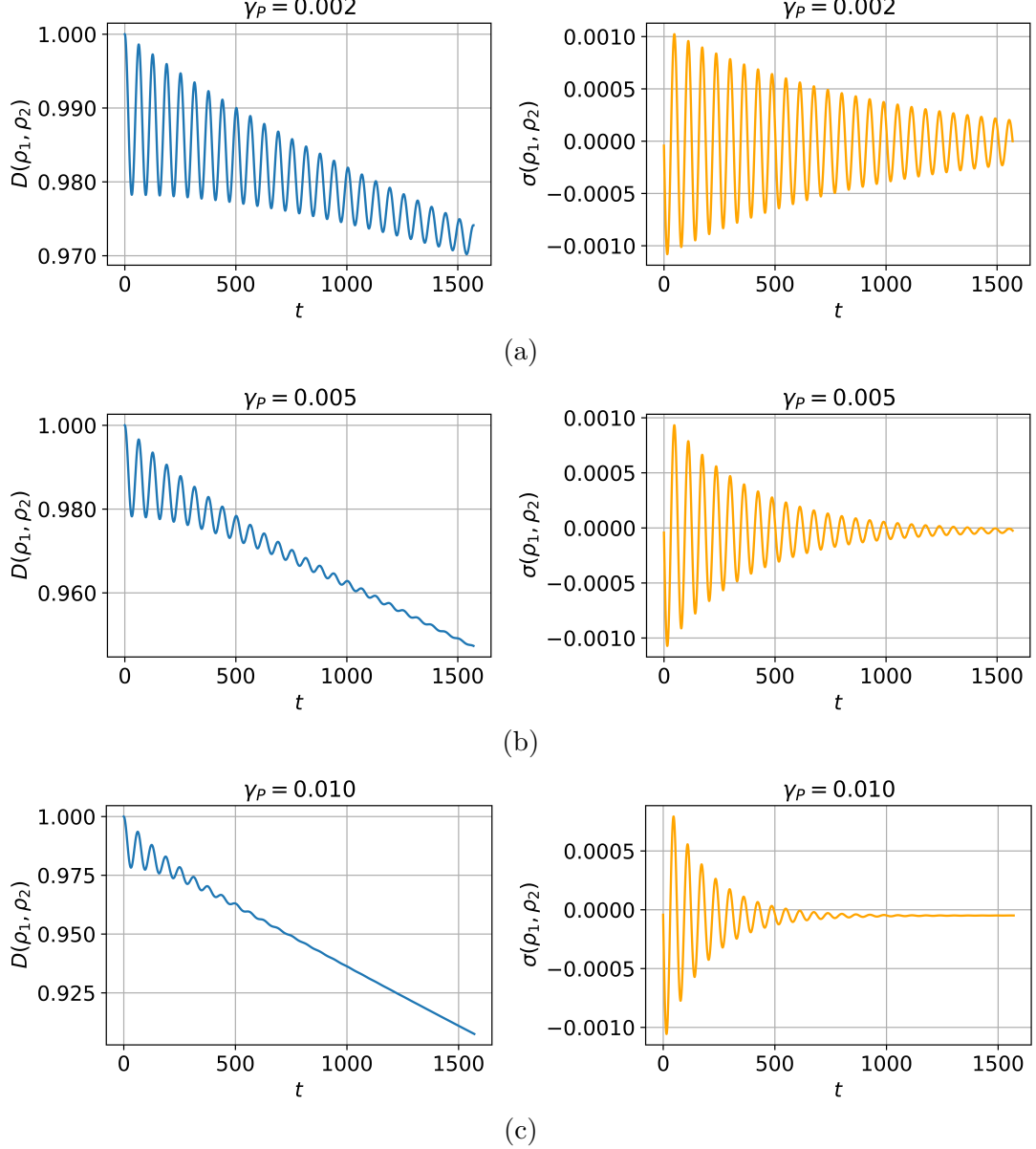


Figure 3.2: Plots of the trace distance  $D$  (left column) and its time derivative  $\sigma$  (right column) as functions of time  $t$  in the presence of motional dephasing during a single MS gate. Subfigures (a), (b), and (c) correspond to the same parameters  $\gamma = 0$ ,  $n_{\text{th}} = 0.05$ , but different dephasing rates  $\gamma_P = 0.002, 0.005, 0.010$ , respectively.

From the left column of Fig. 3.2, it can be seen that oscillations in the trace distance  $D$ —originating from qubit-motion correlations induced by the MS interaction—decay over time. The stronger the dephasing rate  $\gamma_P$ , the faster these oscillations vanish. In addition to the suppression of oscillatory behavior,  $D$  exhibits an overall linear decay with a slope that increases with  $\gamma_P$ . Thus, dissipation induces two

simultaneous effects: (i) a gradual suppression of oscillation amplitude, and (ii) an overall reduction of the baseline value of  $D$ .

The trace distance quantifies the distinguishability between two quantum states and serves as a witness of non-Markovianity. The progressive disappearance of oscillations therefore signals the suppression of non-Markovian features in the qubit evolution. Importantly, this behavior should not be interpreted as a consequence of qubit-motion entanglement alone, but rather as a manifestation of the open-system dynamics governed by dissipation. Since motional heating and dephasing are Markovian processes by construction, they can be described by a Lindblad master equation with time-independent noise operators. The resulting linear decay of  $D$  is fully consistent with the time-independence of the noise.

An interesting feature here is the coexistence of two decay mechanisms: the suppression of oscillations and the negative drift of  $D$ . This raises the question of whether the trace distance is monotonically dependent on the dissipation parameters  $\gamma_P$ , or whether competition between the two decay channels could lead to nontrivial features such as curve crossings. To address this point, Fig. 3.3 compares trace distance across different values of  $\gamma_P$ . The result is unambiguous: the trace distance decreases monotonically with increasing  $\gamma_P$ , with no evidence of curve crossings. Thus, the dependence on the dissipation strength turns out to be trivial, and the two decay mechanisms—oscillation suppression and overall drift—do not compete in a way that produces non-monotonic behavior.

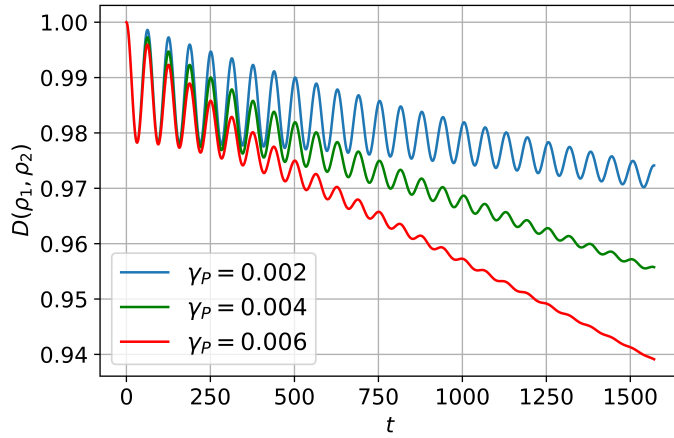


Figure 3.3: Comparison of  $D$  for different values of the dephasing rate  $\gamma_P$ , with other parameters fixed  $n_{\text{th}} = 0.05$ ,  $\gamma = 0$ .

The right column of Fig. 3.2 shows the time derivative  $\sigma$  of the trace distance. We find that  $\sigma$  becomes strictly negative after a finite time  $t_c$ . Moreover, when the dephasing rate is sufficiently large,  $\sigma$  approaches a constant negative value, reflecting the linear decay of  $D$  at long times.

Dissipation does more than simply suppress the non-Markovian oscillations of the qubit dynamics (a process that would otherwise require infinite time). Because dissipation is intrinsically Markovian, it introduces a persistent negative bias in  $\sigma$ . When the non-Markovian contribution from the MS interaction becomes smaller in magnitude than this bias, the dynamics undergoes a crossover: before  $t_c$ , the reduced qubit subsystem evolution remains non-Markovian, whereas beyond  $t_c$ , it

becomes effectively Markovian.

A natural next step is to investigate the dependence of  $t_c$  on dissipation parameters. To this end, one should first establish that  $t_c$  is independent of the choice of initial states. Once this is confirmed,  $t_c$  can be extracted for a broad set of dephasing rates  $\gamma_P$  (with  $n_{\text{th}}$  and  $\gamma$  fixed in a given coupling regime), and fitted to an empirical relation  $t_c(\gamma_P)$ . Such an analysis would provide a quantitative characterization of the non-Markovian-to-Markovian crossover.

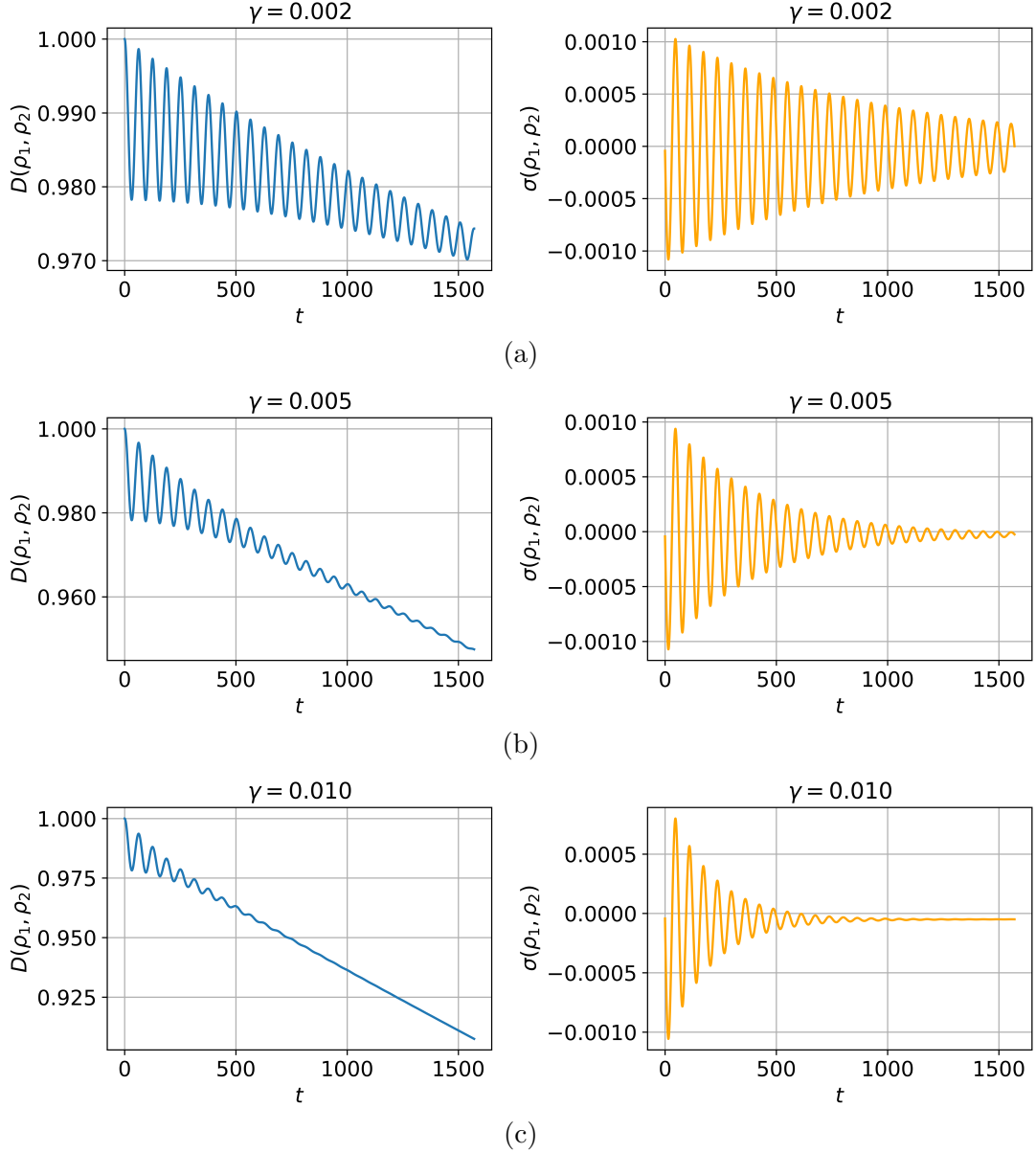


Figure 3.4: Plots of the trace distance  $D$  (left column) and its time derivative  $\sigma$  (right column) as functions of time  $t$  in the presence of motional heating during a single MS gate. Subfigures (a), (b), and (c) correspond to the same parameters  $\gamma_P = 0$ ,  $n_{\text{th}} = 0.05$ , but different heating rates  $\gamma = 0.002, 0.005, 0.010$ , respectively.

In a similar manner, Fig. 3.4 presents the results for the case of pure motional heating. The qualitative features are essentially the same as those observed under

motional dephasing. However, as suggested by Eq. (3.10), quantitative differences are expected to arise at different values of  $n_{\text{th}}$ .

In this section, I investigated how motional dissipation—arising from environmental noise acting on the motional mode—affects the information flow of the qubit subsystem. Dissipation manifests in two main aspects: the reduction of oscillation amplitude in the trace distance  $D$  and its overall downward drift. First, the disappearance of oscillations in  $D$  reflects the progressive suppression of information flow between the qubit and motional modes. This demonstrates that dissipation acts through qubit-motion entanglement to weaken the non-Markovian features of the reduced qubit dynamics. Second, the monotonic decrease of  $D$  introduces a persistent negative bias in  $\sigma(t) = \dot{D}(t)$ . As a result, after a finite time  $t_c$ , the trace distance becomes strictly monotonic and the qubit dynamics is effectively Markovian. Physically, this means that motional dissipation not only reduces the total information of the composite system, but also enables information initially stored in the motional mode to be irreversibly lost through qubit-motion entanglement. This dissipative loss is uniform, leading to the observed negative drift of  $D$ .

# 4

## Noise structure of time miscalibration

### Contents

---

4.1 Decomposition of MS propagator . . . . .	19
4.2 Error channel . . . . .	21

---

Experimental control errors, particularly parameter calibration errors, often prevent the MS gate from being performed successfully, resulting in qubit-motion residual entanglement. Typical examples include time miscalibration, a time error in the gate duration, and symmetric detuning errors, which arise from slow fluctuations or mis-sets in the trap frequency [12].

In this chapter, I focus on the noise structure induced by time miscalibration. I derive an analytical expression for the MS gate under time miscalibration, showing that it can be decomposed into two error gates and an ideal MS gate, thereby elucidating its underlying physical behavior. Furthermore, assuming an initially separable qubit–motion state, I model the effect of time miscalibration as an error channel, that is, a quantum channel specifically capturing the noise introduced by this control imperfection. I then construct the Choi matrix [38] and canonical Kraus operators [39] of the corresponding dynamical map, which reveal a fixed noise structure characteristic of this error.

### 4.1 Decomposition of MS propagator

Recall Eq. (2.12), when Eq. (2.14) is satisfied,  $G(t)$  and  $F(t)$  vanish, which means that no entanglement between the internal state and the motional state is generated. Because time miscalibration originates from the finite precision of experimental control, we consider the case where an absolute time error  $\Delta t$  occurs in the duration of

the MS gate.,

$$t \rightarrow t + \Delta t, \quad |\Delta t| \ll t. \quad (4.1)$$

Then the gate becomes

$$U(t) \rightarrow U(t + \Delta t) = e^{-iF(t+\Delta t)J_yx}e^{-iG(t+\Delta t)J_yp}e^{-iA(t+\Delta t)J_y^2}. \quad (4.2)$$

By explicit expansion, it is found that when  $t$  satisfies Eq. (2.14),  $F(t+\Delta t)$ ,  $G(t+\Delta t)$ , and  $A(t + \Delta t)$  have closed forms

$$\begin{aligned} F(t + \Delta t) &= -\sqrt{2}\frac{\eta\Omega}{\delta}\sin(\delta\Delta t), \\ G(t + \Delta t) &= -\sqrt{2}\frac{\eta\Omega}{\delta}[1 - \cos(\delta\Delta t)], \\ A(t + \Delta t) &= -\frac{\eta^2\Omega^2}{\delta^2}K2\pi - \frac{\eta^2\Omega^2}{2\delta^2}[2\delta\Delta t - \sin(2\delta\Delta t)]. \end{aligned} \quad (4.3)$$

Using these results, the MS propagator with a timing error  $\Delta t$  can be rearranged into a structured form. The rearrangement relies on the commutation relations among the operators and repeated application of the BCH formula. As a result, the propagator can be factorized as

$$U_{\text{MS}}(\Delta t) = V_m(\Delta t)V_q(\Delta t)U_{\text{MS}}, \quad (4.4)$$

with the analytical expression

$$\begin{aligned} V_m(\Delta t) &= e^{i\sqrt{2}\frac{\eta\Omega}{\delta}J_y[\sin(\delta\Delta t)x+(1-\cos(\delta\Delta t))p]}, \\ V_q(\Delta t) &= e^{i\frac{\eta^2\Omega^2}{\delta^2}J_y^2[\delta\Delta t-\sin(\delta\Delta t)]}, \\ U_{\text{MS}} &= \exp[i\frac{\pi}{4}\sigma_y^{(1)}\sigma_y^{(2)}]. \end{aligned} \quad (4.5)$$

In Eq. (4.5),  $V_m$  can be interpreted as the error gate induced by entanglement with the motional mode. Physically, it corresponds to unwanted qubit-motion residual entanglement. This can be seen directly from the analytical expression as in the expression the  $J_y \otimes x$  and  $J_y \otimes p$  tensor product terms do not vanish.  $V_q$  is the error gate induced by an effective additional spin-spin interaction, independently of the motional state, since there is only an additional  $J_y^2$ . And  $U_{\text{MS}}$  is the noiseless MS gate.

The qubit-motion residual entanglement can be visualized directly in the phase-space schematic diagram, as shown in Fig. 4.1. To characterize the absolute time error, I introduce a dimensionless parameter

$$\gamma_t \equiv \delta\Delta t/2\pi, \quad (4.6)$$

which quantifies the deviation of the phase-space circular trajectory from perfect closure.

In the ideal case  $\gamma_t = 0$ , the circular trajectory closes exactly, and no residual entanglement remains between the qubits and motional state. By contrast, when

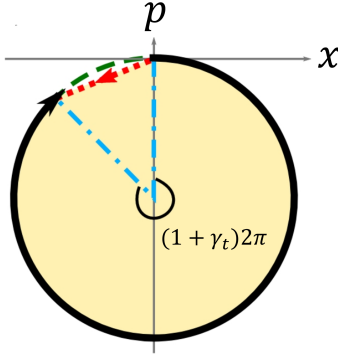


Figure 4.1: Phase-space schematic diagram of the MS gate under time miscalibration.

a time error is present,  $\gamma_t$  does not vanish, the circular trajectory fails to close, resulting in qubit-motion residual entanglement.

Studying the MS gate under time miscalibration is instructive, as it induces effects analogous to those of the symmetric detuning error. In fact, the same dimensionless parameter  $\gamma_t$  can be used to characterize both cases, since  $\delta$  and  $t$  enter Eq. (4.6) on an equal footing. In either case, the imperfect parameter setting results in a phase error, causing the phase-space trajectory to remain open and thereby leaving residual qubit-motion entanglement.

## 4.2 Error channel

To characterize the effective quantum channel associated with the noise, a common approach is to construct its Choi state, defined as [38]

$$\mathcal{J}(\mathcal{N}) = (\mathcal{N}_{A \rightarrow B} \otimes I_R)(|\Phi\rangle\langle\Phi|_{AR}), \quad |\Phi\rangle_{AR} = \sum_i |ii\rangle_{AR}, \quad (4.7)$$

where  $\mathcal{N}_{A \rightarrow B}$  is the effective quantum channel and  $R$  is a reference system of the same dimension as the input system  $A$ . Here  $|\Phi\rangle_{AR}$  denotes the unnormalised maximally entangled state on  $AR$ , defined with respect to some orthonormal basis  $\{|i\rangle\}_A$ ,  $\{|j\rangle\}_R$  of  $\mathcal{H}_A$  and  $\mathcal{H}_R$ , respectively.

In the present case, the situation is slightly more involved. Since the MS gate acts jointly on the qubit and motional degrees of freedom, the effective map on the qubit subsystem necessarily involves both tensoring with the motional state and subsequently tracing it out. To construct the Choi state, we prepare the four-qubit input state  $|\psi\rangle = \frac{1}{2}(|0000\rangle + |0101\rangle + |1010\rangle + |1111\rangle)$ , apply the MS gate to the first two qubits, and then trace over the motion. The resulting reduced qubit state,

$$\begin{aligned} \rho_{q,out} &= (\mathcal{N}_{q1,q2} \otimes I_{q3,q4})[\rho_{q,in}] \\ &\equiv \text{Tr}_m \left[ U_{\text{MS}}(\Delta t) \otimes I_{q3,q4} (\rho_{q,in} \otimes \rho_m) U_{\text{MS}}^\dagger(\Delta t) \otimes I_{q3,q4} \right] \end{aligned} \quad (4.8)$$

is the Choi state  $\mathcal{J}(\mathcal{N})$  of the dynamical map  $\mathcal{N}_{q1,q2}$ .

By exploiting the ensemble decomposition of the Choi state, one can construct

a minimal set of canonical Kraus operators  $K'_i$  [38, 39]. In our case, since the MS gate under time miscalibration is modeled as an error channel acting after an ideal MS gate, and the ideal MS gate is independent of the motional quantum number, the corresponding canonical Kraus operators  $K_i$  are obtained by multiplying the obtained operators with the adjoint of the ideal propagator,

$$K_i = K'_i U_{\text{MS}}^\dagger. \quad (4.9)$$

By examining the canonical Kraus operators in their matrix representation, as shown in Fig. 4.2, I observe that the distribution of their matrix elements exhibits a fixed and structured pattern. Remarkably, although the quantum channel depends on the motional state, the positions of the nonzero entries remain invariant, regardless of variations in the mean phonon number of the motional state or the magnitude of the error. This invariance indicates the existence of an intrinsic and parameter-independent noise structure associated with time miscalibration in the MS gate.

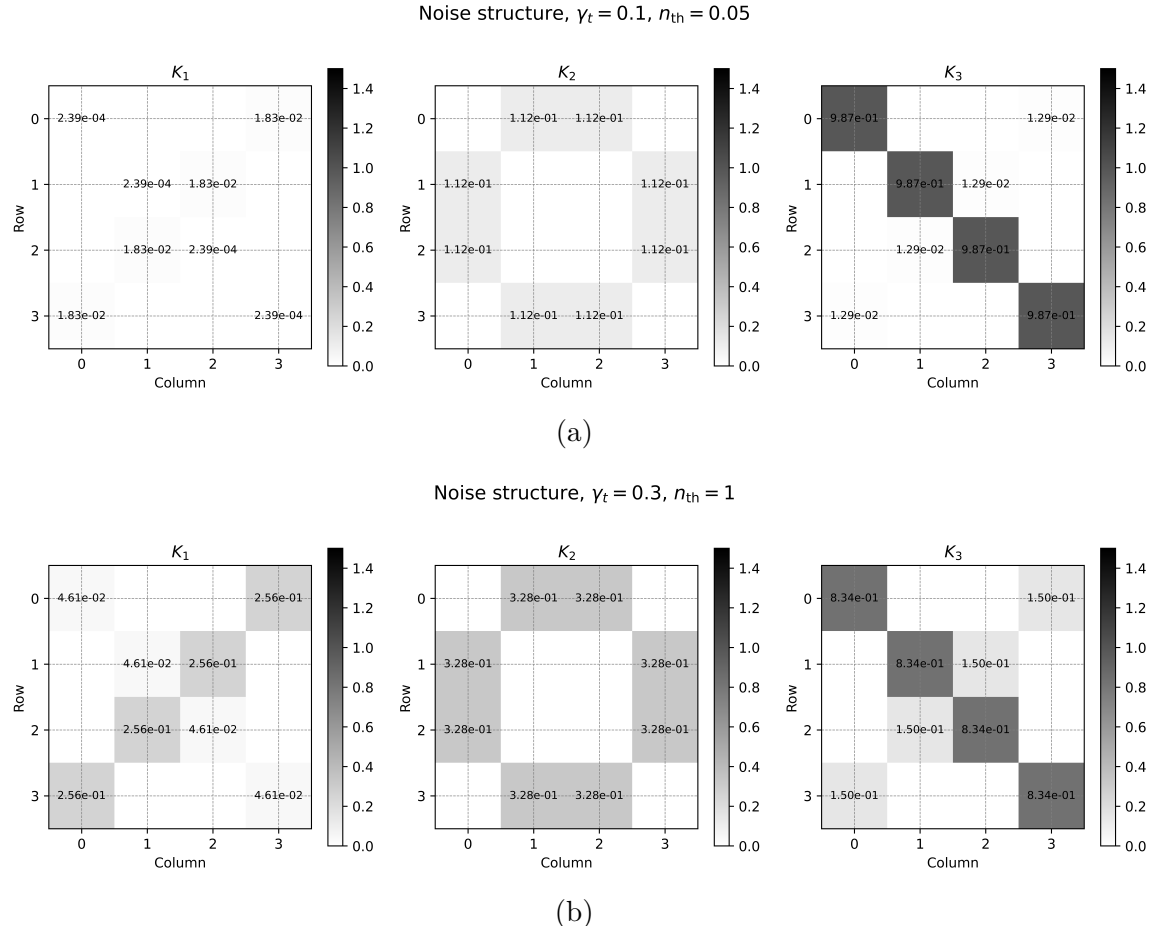


Figure 4.2: Heatmaps of the magnitude of matrix elements of canonical Kraus operators with (a)  $\gamma_t = 0.1, n_{\text{th}} = 0.05$  and (b)  $\gamma_t = 0.3, n_{\text{th}} = 1$ . White regions without numerical values correspond to matrix elements that vanish within numerical precision.

The canonical Kraus operators can be expanded in the Pauli operator basis, with

coefficients  $c_{kl} = \frac{1}{4}\text{Tr}\left[K(\sigma_k^\dagger \otimes \sigma_l^\dagger)\right]$ . By projecting each Kraus operator onto the Pauli basis and retaining only the non-vanishing components, its algebraic structure can be explicitly identified as

$$\begin{aligned} K_1 &= c_1 I + c_2 \sigma_y^{(1)} \sigma_y^{(2)}, \\ K_2 &= c_3 (\sigma_y^{(1)} I + I \sigma_y^{(2)}), \\ K_3 &= c_4 I + c_5 \sigma_y^{(1)} \sigma_y^{(2)}. \end{aligned} \quad (4.10)$$

Equivalently, in terms of the collective operator  $J_y$ , the canonical Kraus operators take the form

$$\begin{aligned} K_1 &= a_1 I + a_3 J_y^2, \\ K_2 &= k_2 J_y, \\ K_3 &= a_2 I + a_4 J_y^2, \end{aligned} \quad (4.11)$$

where the coefficients  $\{a_i, k_2\}$  depend on the gate parameters and the noise level.

By inspection, the sign of  $\gamma_t$  affects only the sign of the imaginary part of  $a_{1,2,3,4}$ , while leaving their magnitudes unchanged. The dependence of the coefficients on system parameters is summarized in Table 4.1. As shown, the coefficients are sensitive to both the time miscalibration parameter  $\gamma_t$  and the mean phonon number  $n_{\text{th}}$ . With increasing noise level (either larger  $\gamma_t$  or larger  $n_{\text{th}}$ ), the magnitude of  $|a_2|$  decreases slightly from unity, whereas the other coefficients systematically grow, indicating the enhanced contribution of error terms.

Table 4.1: Magnitudes of coefficients  $\{|a_1|, |a_3|, |k_2|, |a_2|, |a_4|\}$  for different values of time miscalibration  $\gamma_t$  and mean phonon number  $n_{\text{th}}$ .

$(\gamma_t, n_{\text{th}})$	$ a_1 $	$ a_3 $	$ k_2 $	$ a_2 $	$ a_4 $
(0.1, 0.00)	0.016	0.033	0.213	1.000	0.024
(0.1, 0.05)	0.018	0.037	0.223	1.000	0.026
(0.1, 1.00)	0.046	0.095	0.352	0.999	0.064
(0.3, 0.00)	0.098	0.211	0.490	0.995	0.170
(0.3, 0.05)	0.106	0.230	0.507	0.994	0.177
(0.3, 1.00)	0.213	0.512	0.656	0.977	0.300

Notably, the time miscalibration shares the same canonical Kraus operators as the motional dephasing case in Eq. (2.20), with the coefficients determined by the dephasing rate and system parameters. However, unlike motional dephasing, it does not admit a similar reshaping process [25]. This limitation arises from the gap between theory and experiment, as discussed in the Introduction: the presence of qubit-motion residual entanglement in experiments prevents the same QEC circuit from reshaping this structure into a useful form of noise. And why these two cases exhibit the same Kraus structure remains an open question.

# 5

## Non-CP maps from time-miscalibrated MS gates

### Contents

---

5.1	Circuit model and the definition of the map . . . . .	25
5.2	The linearity of the effective map . . . . .	26
5.3	Constructing the effective map . . . . .	27
5.4	The region of the non-CP map in parameter space . . . .	29
5.5	The effect of motional dissipation . . . . .	31

---

The reduced dynamics of a quantum system in contact with an environment is guaranteed to be completely positive (CP) if product initial conditions are assumed. However, for correlated initial conditions, this need not hold [26]. When the motional degree of freedom of the trapped-ion system is regarded as the environment, it naturally follows that qubit-motion correlations not only govern the flow of information between the two subsystems, but can also be exploited to construct initial states with correlations. This raises fundamental questions: under such conditions, does the reduced qubit dynamics necessarily lose complete positivity? Or under what conditions does it become non-CP? Addressing these questions may not only offer a new approach for engineering non-Markovian dynamics through non-CP maps, but also provide fresh insights into the fundamental relationship between correlations and non-CP maps.

After deriving the analytical expression for the MS gate under time miscalibration, I found that the tunable parameter  $\gamma_t$  directly controls the strength of qubit-motion residual entanglement. This tunable entanglement, in turn, serves as a handle for engineering correlated initial states: by varying  $\gamma_t$ , one can systematically control the initial state preparation and thereby identify those that give rise to non-CP reduced dynamics.

In this chapter, I present a framework for constructing non-CP maps in this man-

ner, and use it to investigate both the conditions for their existence and the feasibility of generating non-Markovian dynamics by concatenating such maps. Concretely, I design a simple circuit consisting of two MS gates with time miscalibration, characterized by two tunable parameters. The first gate is used to prepare a correlated qubit-motion initial state, while the second gate defines an effective map acting on the qubits. I rigorously prove that this effective map is necessarily linear, which allows me to construct it via the Pauli transfer matrix representation and to compute its Choi matrix [40, 41], the latter providing the criterion for complete positivity. I then perform a grid search over the parameter space to identify the regions where the map is non-CP and visualize the degree of deviation from complete positivity. Finally, I analyze how motional dissipation influences the conditions under which non-CP maps emerge.

## 5.1 Circuit model and the definition of the map

As shown in Fig. 5.1, the quantum circuit under consideration consists of two consecutive MS gates subject to timing errors  $\Delta t_1$  and  $\Delta t_2$ , which we parametrize as  $\gamma_{t1}$  and  $\gamma_{t2}$  according to Eq. (4.6).

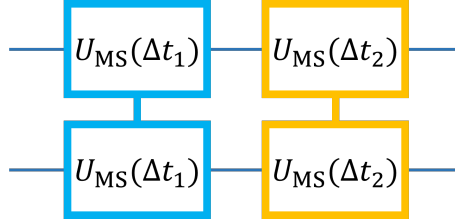


Figure 5.1: Quantum circuit model with two MS gate under time miscalibration with timing error  $\Delta t_1$  and  $\Delta t_2$ .

In Fig. 5.1, the first gate is used to construct an intermediate state with qubit-motion residual entanglement. At the circuit input the global state is taken to be a separable state  $\rho_{q,0} \otimes \rho_m$ , where  $\rho_{q,0}$  denotes the initial two-qubit state and  $\rho_m$  the motional state. Under this assumption the reduced qubit map induced by the first gate,

$$\mathcal{N}_1[\rho_{q,0}] \equiv \text{Tr}_m \left[ U_{\text{MS}}(\Delta t_1) \rho_{q,0} \otimes \rho_m U_{\text{MS}}^\dagger(\Delta t_1) \right] \quad (5.1)$$

is a completely positive, trace-preserving (CPTP) map by construction. Likewise, the overall reduced dynamics produced by the two gates acting in sequence,

$$\mathcal{N}_2[\rho_{q,0}] \equiv \text{Tr}_m \left[ U_{\text{MS}}(\Delta t_2) U_{\text{MS}}(\Delta t_1) \rho_{q,0} \otimes \rho_m U_{\text{MS}}^\dagger(\Delta t_1) U_{\text{MS}}^\dagger(\Delta t_2) \right]. \quad (5.2)$$

is also CPTP when viewed as a map from the original product input.

The central object of interest for this circuit, however, is the effective map that takes the qubit state immediately before the second gate (the output of  $\mathcal{N}_1$ ) to the qubit state after the second gate (the output of  $\mathcal{N}_2$ ):

$$\mathcal{N} : \mathcal{N}_1[\rho_{q,0}] \mapsto \mathcal{N}_2[\rho_{q,0}] \quad (5.3)$$

Because the first MS gate under time miscalibration generically creates qubit-motion correlations, the joint state immediately prior to the second gate is in general not factorizable. Explicitly, after the first time-miscalibrated MS gate the joint qubit-motion state reads  $\rho'_{qm} = U_{MS}(\Delta t_1) (\rho_{q,0} \otimes \rho_m) U_{MS}^\dagger(\Delta t_1)$ , and the corresponding reduced qubit state is  $\rho'_q = \text{Tr}_m(\rho'_{qm})$ . The final qubit state produced by the second gate is therefore  $\rho_{q,out} = \text{Tr}_m[U_{MS}(\Delta t_2) \rho'_{qm} U_{MS}^\dagger(\Delta t_2)]$ .

Thus, in comparison with Eq. (5.3), the effective map can be expressed in a more transparent form as

$$\mathcal{N} : \rho'_q \longmapsto \rho_{q,out}, \quad (5.4)$$

which explicitly emphasizes that the effective dynamics is defined as a transformation from the intermediate reduced qubit state  $\rho'_q$  to the final reduced state  $\rho_{q,out}$ .

The crucial subtlety is that the correlated intermediate state  $\rho'_{qm}$  does not, in general, factorize as  $\rho'_q \otimes \rho_m$ . Equivalently, the motional state entering the second gate depends on the prior qubit input  $\rho_{q,0}$ . Because of this dependence, there is no guarantee that a single, state-independent CPTP map  $\mathcal{N}$  exists for every possible  $\rho'_q$ . In other words, the map from the intermediate reduced state to the final reduced state may fail to be CP: the motional state retains memory of the qubit subsystem, thereby violating the assumption of an input-independent environment that underlies the usual CPTP description.

This reasoning also clarifies the precise sense in which the theoretical circuit model deviates from experimental reality. In the idealized quantum-circuit picture, each gate is represented as a CPTP map acting solely on the qubit Hilbert space. The intermediate state after the first gate is then modeled as  $\rho'_q \otimes \rho_m$ , so that the motional degree of freedom is treated as a fixed environment, independent of the qubit input. In this case, the final qubit state takes the form

$$\rho_{q,out}^{\text{theory}} = \text{Tr}_m \left[ U_{MS}(\Delta t_2) (\rho'_q \otimes \rho_m) U_{MS}^\dagger(\Delta t_2) \right], \quad (5.5)$$

which by construction always corresponds to a CPTP map on the qubits.

In the experimental setting, however, the true intermediate state is the correlated  $\rho'_{qm}$ , not a separable state. Consequently, the second gate acts on a system-environment state whose environmental part encodes information about earlier qubit dynamics. The resulting reduced dynamics can therefore deviate from complete positivity and exhibit memory effects, revealing physical behavior that is invisible to the qubit-only circuit abstraction.

## 5.2 The linearity of the effective map

Although I have abstractly defined the effective map, its mathematical properties remain to be clarified. To investigate them, it is natural to begin with what can be directly deduced from its definition. According to Eq. (5.3), the input and output states that specify this map are well defined. Moreover, since both  $\mathcal{N}_1$  and  $\mathcal{N}_2$  are CPTP maps, they are guaranteed to possess linearity, complete positivity, and trace preservation. I therefore start by examining the linearity of the effective map.

Consider a general initial state of the circuit of the form

$$\rho_{q,0} = p\rho_{q1,0} + (1-p)\rho_{q2,0}, \quad 0 \leq p \leq 1, \quad (5.6)$$

which represents a classical mixture of two states  $\rho_{q1,0}$  and  $\rho_{q2,0}$ .

From the definition of  $\mathcal{N}$ , the following chain of equalities can be established:

$$\begin{aligned} \mathcal{N}[\mathcal{N}_1[\rho_{q,0}]] &= \mathcal{N}_2[\rho_{q,0}], \\ \mathcal{N}[p\mathcal{N}_1[\rho_{q1,0}] + (1-p)\mathcal{N}_1[\rho_{q2,0}]] &= p\mathcal{N}_2[\rho_{q1,0}] + (1-p)\mathcal{N}_2[\rho_{q2,0}], \\ \mathcal{N}[p\mathcal{N}_1[\rho_{q1,0}] + (1-p)\mathcal{N}_1[\rho_{q2,0}]] &= p\mathcal{N}[\mathcal{N}_1[\rho_{q1,0}]] + (1-p)\mathcal{N}[\mathcal{N}_1[\rho_{q2,0}]]. \end{aligned} \quad (5.7)$$

Here, the left-hand side of the second equality follows from the linearity of  $\mathcal{N}_1$ , while the right-hand side exploits the linearity of  $\mathcal{N}_2$ . In the third equality, we once again invoke the definition of  $\mathcal{N}$ . Since the initial qubit state  $\rho_{q,0}$  was chosen to be an arbitrary convex combination, this argument establishes that the effective map  $\mathcal{N}$  is universally linear.

Having rigorously established that the effective map  $\mathcal{N}$  is linear, one can represent it in the Pauli transfer matrix formalism, which provides a convenient and systematic way to explicitly construct the map.

Next, we examine its trace preservation and positivity properties. From Eq. (5.6), any valid density operator  $\rho_{q,0}$  has unit trace. Since both  $\mathcal{N}_1$  and  $\mathcal{N}_2$  are trace-preserving maps, we have  $\text{Tr}(\mathcal{N}_1[\rho_{q,0}]) = \text{Tr}(\mathcal{N}_2[\rho_{q,0}]) = 1$ . Consequently, for any initial state, the input and output of  $\mathcal{N}$  must have identical trace, implying that the effective map itself is trace preserving.

Turning to positivity, recall that a positive map is defined as one that takes any positive semi-definite operator to another positive semi-definite operator. Strictly speaking, our effective map  $\mathcal{N}$  is only defined on the set of physical density operators (i.e., positive semi-definite, unit-trace operators), rather than on arbitrary operators. Nevertheless, within this physically relevant domain we can still argue positivity: since any initial qubit state  $\rho_{q,0}$  is a positive semi-definite density operator, and both  $\mathcal{N}_1$  and  $\mathcal{N}_2$  are themselves positive maps, it follows that the input state  $\mathcal{N}_1[\rho_{q,0}]$  and the corresponding output  $\mathcal{N}_2[\rho_{q,0}]$  must always remain positive semi-definite. Therefore, by construction, the effective map  $\mathcal{N}$  maps every valid density operator to another valid density operator, ensuring positivity on its natural domain of definition.

## 5.3 Constructing the effective map

Having rigorously proved that the effective map  $\mathcal{N}$  is linear, I can proceed to its explicit construction.

In order to uniquely determine a linear map acting on two qubits, one must specify its action on a basis of operators that spans the operator space. Since the operator space of a  $d$ -dimensional system has dimension  $d^2$ , the two-qubit case ( $d = 4$ ) requires  $d^2 = 16$  linearly independent density operators to uniquely fix the map. So I need to prepare 16 linearly independent initial states at the circuit input.

The overall construction procedure is as follows:

1. Prepare 16 linearly independent physical two-qubit initial states  $\rho_0^{(\nu)}$ .
2. For each  $\rho_0^{(\nu)}$ , obtain the intermediate state  $\rho_{\text{in}}^{(\nu)}$  according to Eq. (5.1) and the corresponding output state  $\rho_{\text{out}}^{(\nu)}$  according to Eq. (5.2).
3. Expand both  $\rho_{\text{in}}^{(\nu)}$  and  $\rho_{\text{out}}^{(\nu)}$  in the Pauli operator basis and convert them into 16-component Pauli vectors  $\vec{c}_{\text{in}}^{(\nu)}$  and  $\vec{c}_{\text{out}}^{(\nu)}$ .
4. Solve the linear system  $\vec{c}_{\text{out}}^{(\nu)} = R \vec{c}_{\text{in}}^{(\nu)}$  to obtain the Pauli transfer matrix  $R$  [40] characterizing  $\mathcal{N}$ .
5. Construct the Choi matrix from  $R$  [41] and analyze the complete positivity of the effective map.

To explicitly construct a complete set of linearly independent inputs, we begin with the single-qubit case. A convenient choice of four linearly independent states is given by the computational basis states  $|0\rangle$  and  $|1\rangle$ , together with the equal superposition state  $(|0\rangle + |1\rangle)/\sqrt{2}$  and the phase superposition state  $(|0\rangle + i|1\rangle)/\sqrt{2}$ . By taking tensor products of these four states across two qubits, we obtain 16 two-qubit product states that form a linearly independent set and hence span the entire two-qubit operator space.

At the circuit input we therefore prepare these 16 two-qubit product states, which, after passing through the first time-miscalibrated MS gate, are mapped to 16 intermediate reduced qubit states. It is important to emphasize that although the map  $\mathcal{N}_1$  induced by this gate involves both qubit-motion residual entanglement and a partial trace, and is therefore in general non-invertible, it nevertheless remains a linear map. Consequently, the transformation from the 16 linearly independent input states to the 16 intermediate reduced states consists solely of linear operations and thus preserves their linear independence. Indeed, the fact that the system of linear equations used to construct the Pauli transfer matrix  $R$  always admits a solution is itself a reflection of this preserved independence. These 16 states therefore constitute an informationally complete set, sufficient to uniquely determine the effective map.

Having obtained the input states  $\rho_{\text{in}}^{(\nu)}$  and their corresponding output states  $\rho_{\text{out}}^{(\nu)}$ , the next step is to represent them in a basis that makes the action of the effective map  $\mathcal{N}$  transparent. The two-qubit Pauli operator basis is particularly advantageous for this purpose: it provides a complete operator basis, has direct physical interpretation in terms of Pauli observables, and leads to a compact description of the map in the form of a Pauli transfer matrix. In this representation, any density operator can be expanded as a linear combination of Pauli operators, with the coefficients collected into a vector that encodes the operator in a convenient and structured way.

Any two-qubit density operator can thus be expanded in the Pauli basis as

$$\rho = \frac{1}{4} \sum_{ij} c_{ij} (\sigma_i \otimes \sigma_j), \quad i, j = 0, \dots, 3, \quad (5.8)$$

with the corresponding Pauli vector

$$\vec{c} = [c_{00}, c_{01}, \dots, c_{33}]^T, \quad c_{ij} = \text{Tr}[(\sigma_i \otimes \sigma_j)\rho]. \quad (5.9)$$

In this Pauli representation, the effective map  $\mathcal{N}$  reduces to a linear transformation between Pauli vectors, described by the Pauli transfer matrix  $R$ , which greatly

facilitates the analysis of trace preservation and complete positivity.

For each input-output pair, the corresponding Pauli vectors satisfy the linear relation

$$\vec{c}_{\text{out}}^{(\nu)} = R \vec{c}_{\text{in}}^{(\nu)}, \quad \nu = 1, 2, \dots, 16. \quad (5.10)$$

By stacking the 16 input vectors as columns of a matrix  $M_{\text{in}} = [\vec{c}_{\text{in}}^{(1)}, \vec{c}_{\text{in}}^{(2)}, \dots, \vec{c}_{\text{in}}^{(16)}]$  and similarly for  $M_{\text{out}}$ , the Pauli transfer matrix  $R$  can be obtained by linear inversion,

$$R = M_{\text{out}} \cdot M_{\text{in}}^{-1}. \quad (5.11)$$

Once the map has been constructed in this way, one can immediately verify its trace-preserving property by examining the first row of  $R$ , which directly encodes conservation of the trace.

Having thus established a concrete representation of the effective map and a straightforward test of its trace preservation, we can proceed to a deeper structural analysis. In particular, by exploiting the well-known correspondence between the Pauli transfer matrix and the Choi matrix, one can directly check whether the map is completely positive.

From the Pauli transfer matrix  $R$ , the Choi matrix is constructed as [41]

$$\mathcal{J}(\mathcal{N}) = \frac{1}{d} \sum_{\mu\nu} R_{\mu\nu} P_\mu \otimes P_\nu^T, \quad (5.12)$$

where  $\{P_\mu\}$  is the two-qubit Pauli operator basis and  $d = 4$  is the Hilbert space dimension of the two-qubit system. According to the complete positivity criterion [38]

$$\mathcal{N} \text{ is CP} \Leftrightarrow \mathcal{J}(\mathcal{N}) \geq 0, \quad (5.13)$$

the map is completely positive if and only if its Choi matrix is positive semi-definite.

In addition, to quantify the degree of deviation from complete positivity in a continuous manner, I introduce the measure

$$\Lambda = \begin{cases} 0, & \lambda_{\min} \geq 0, \\ \lg(1 - \lambda_{\min}), & \lambda_{\min} < 0, \end{cases} \quad (5.14)$$

where  $\lambda_{\min}$  denotes the minimum eigenvalue of the Choi matrix. By definition,  $\Lambda = 0$  for CP maps, while increasingly negative values of  $\lambda_{\min}$  correspond to larger  $\Lambda$ , i.e., a stronger deviation from complete positivity. This measure circumvents the difficulty of directly interpreting the scale of  $\lambda_{\min}$ , whose variations across different orders of magnitude would otherwise fail a consistent characterization.

## 5.4 The region of the non-CP map in parameter space

Based on the circuit shown in Fig. 5.1 and following the procedure outlined above for constructing the effective map, I scan the two parameters  $\gamma_{t1}$  and  $\gamma_{t2}$  to determine whether the resulting map is CP or non-CP. A grid search over the  $(\gamma_{t1}, \gamma_{t2})$  param-

eter space is performed, and for each point the effective map is analyzed to identify regions of non-CP behavior. The degree of deviation from complete positivity is quantified by  $\Lambda$  and visualized as a heatmap.

The resulting distribution of deviations across parameter space is shown in Fig. 5.2. The brown regions correspond to  $\Lambda = 0$ , indicating that the effective map remains CP. By contrast, greener regions correspond to increasing values of  $\Lambda$ , i.e., stronger deviations from CP and thus non-CP behavior. The maximum observed value of  $\Lambda$  lies in the range  $0.05 \sim 0.06$ , which corresponds to a minimum eigenvalue of the Choi matrix on the order of  $-10^{-1}$ .

In addition, the scan over  $\gamma_{t1}$  covers its full range, namely  $\gamma_{t1} \in [-0.5, 0.5]$  (equivalently  $[0, 1]$ ), which reflects the periodicity of the closed-form expressions  $F(t + \Delta t)$ ,  $G(t + \Delta t)$ , and  $A(t + \Delta t)$  in Eq. (4.3) together with the definition of  $\gamma_{t1}$  in Eq. (4.6). In contrast, the range of  $\gamma_{t2}$  is restricted to  $[-0.18, 0.18]$ , which is mainly where non-CP maps occur. Outside this window the map is entirely CP. Also, the region of non-CP behavior exhibits exact central symmetry in the parameter space.

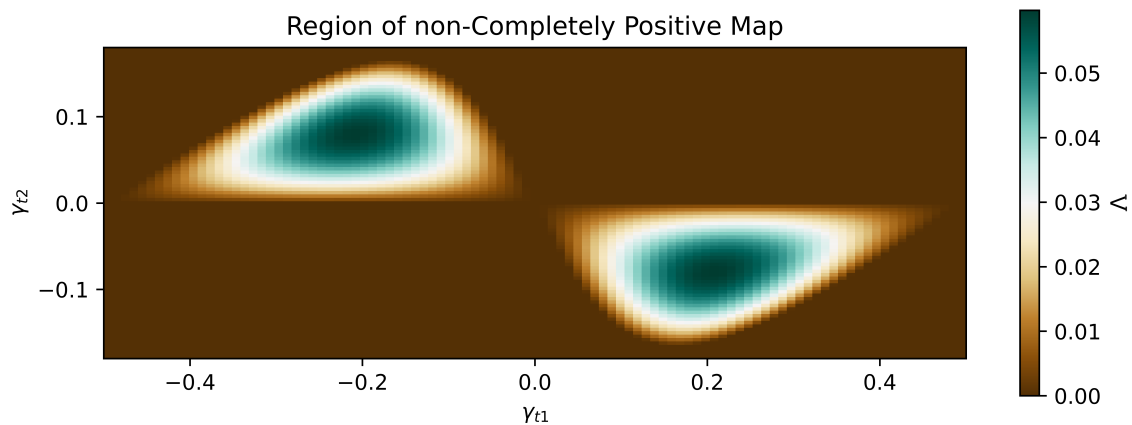


Figure 5.2: Heatmap of the deviation from complete positivity in the parameter space of the effective map. The simulation is performed in the general field coupling regime with parameters  $\eta = 0.1$ ,  $\delta = 0.05\nu$ ,  $\Omega = 0.177\nu$ , and  $n_{\text{th}} = 0.05$ . The horizontal axis corresponds to  $\gamma_{t1} \in [-0.5, 0.5]$ , and the vertical axis to  $\gamma_{t2} \in [-0.18, 0.18]$ . Brown regions indicate  $\Lambda = 0$  (CP maps), while greener regions indicate stronger deviations from CP (non-CP maps).

In Fig. 5.2, the boundary of the non-CP region is described by a nonlinear curve. The largest value of  $\gamma_{t2}$  that still exhibits non-CP behavior is  $1/6$ , corresponding to the points  $(1/6, -1/6)$  and  $(-1/6, 1/6)$ . Remarkably, this value of  $1/6$  is exact. Each non-CP region is enclosed by three special points and the nonlinear curves connecting them. For instance, in the case  $\gamma_{t1} > 0$ , the three defining points are  $(0,0)$ ,  $(0.5,0)$ , and  $(1/6, -1/6)$ . These structural features strongly suggest that the geometry of the non-CP region is determined by an underlying mathematical relation.

Throughout the entire parameter space, the deviation  $\Lambda$  varies smoothly and reaches its maximum at the center of each nonlinear-shaped region. If visualized in three dimensions, the landscape would resemble two symmetric peaks, with the deviation rising from the periphery toward the central maxima.

Notably, Fig. 5.2 reveals that non-CP behavior arises only when the two miscalibration parameters  $\gamma_{t1}$  and  $\gamma_{t2}$  have opposite signs. This observation indicates that

the existence of a non-CP effective map is subject to nontrivial constraints, rather than occurring for arbitrary parameter choices. One such constraint, clearly visible here, is that the two MS gates must be miscalibrated in opposite directions. A second observation is that when  $\gamma_{t2} = 0$ , the effective map is always CP, regardless of the value of  $\gamma_{t1}$  within the range  $[-0.5, 0.5]$ . In other words, even if the intermediate qubit-motion state carries residual entanglement, the reduced qubit dynamics remains completely positive as long as the second MS gate is ideal. The same holds true when both gates are miscalibrated in the same direction.

These cases suggest a general principle: although the motional state retains memory of the qubit subsystem, this memory does not necessarily compromise complete positivity. If the subsequent MS gate does not channel back the stored information from the motion into the qubit, the reduced dynamics remains CP. By contrast, when the second MS gate channels back motional information under specific constraints, the dynamics can violate complete positivity.

This insight resonates with the dynamical picture of MS gates as loops in phase space. Recall Fig. 3.1, each loop corresponds to a process in which information flows from the qubit into the motion and then potentially back to the qubit. It is well established that whenever information flows back from the environment into the system, the dynamics is non-Markovian. Since non-Markovian dynamics can often be decomposed into segments governed by non-CP maps, our results suggest that the non-CP condition observed here might be understood from an information theory perspective. Specifically, the emergence of non-CP behavior signals parameter regions where stored motional information flows back into the qubit.

Taken together, these results reveal a close connection between non-CP maps, non-Markovianity, and information backflow. While the present analysis does not yet establish a formal equivalence, it strongly motivates further study along this direction. In particular, one promising line of research is to characterize the effective map not only in terms of its complete positivity, but also by analyzing the associated information flow within the circuit. Such an approach could provide a unified framework for connecting non-CP reduced dynamics with the broader theory of non-Markovian processes.

Beyond these foundational considerations, there is also a practical direction to pursue. By deliberately introducing a controlled timing bias to the MS gate, the system can be tuned to regions of parameter space where the deviation from complete positivity is maximized, thereby enabling the systematic construction of non-CP maps. If the circuit is regarded as a single time step, then repeating such biased gates over multiple steps naturally generates a simulation of non-Markovian dynamics. In more realistic experimental settings, however, additional factors such as dissipation must be taken into account. Thus, in the following section I will explore how motional dissipation modifies the parameter-space region in which non-CP maps emerge.

## 5.5 The effect of motional dissipation

Motional dissipation constitutes the dominant source of decoherence in trapped-ion quantum platforms. To investigate its impact on the emergence of non-CP maps,

we include the motional dephasing channel described in Eq. (3.10) and evaluate how it modifies the results obtained in the dissipation-free case. The dynamics are simulated using the `mesolve` function in QuTiP.

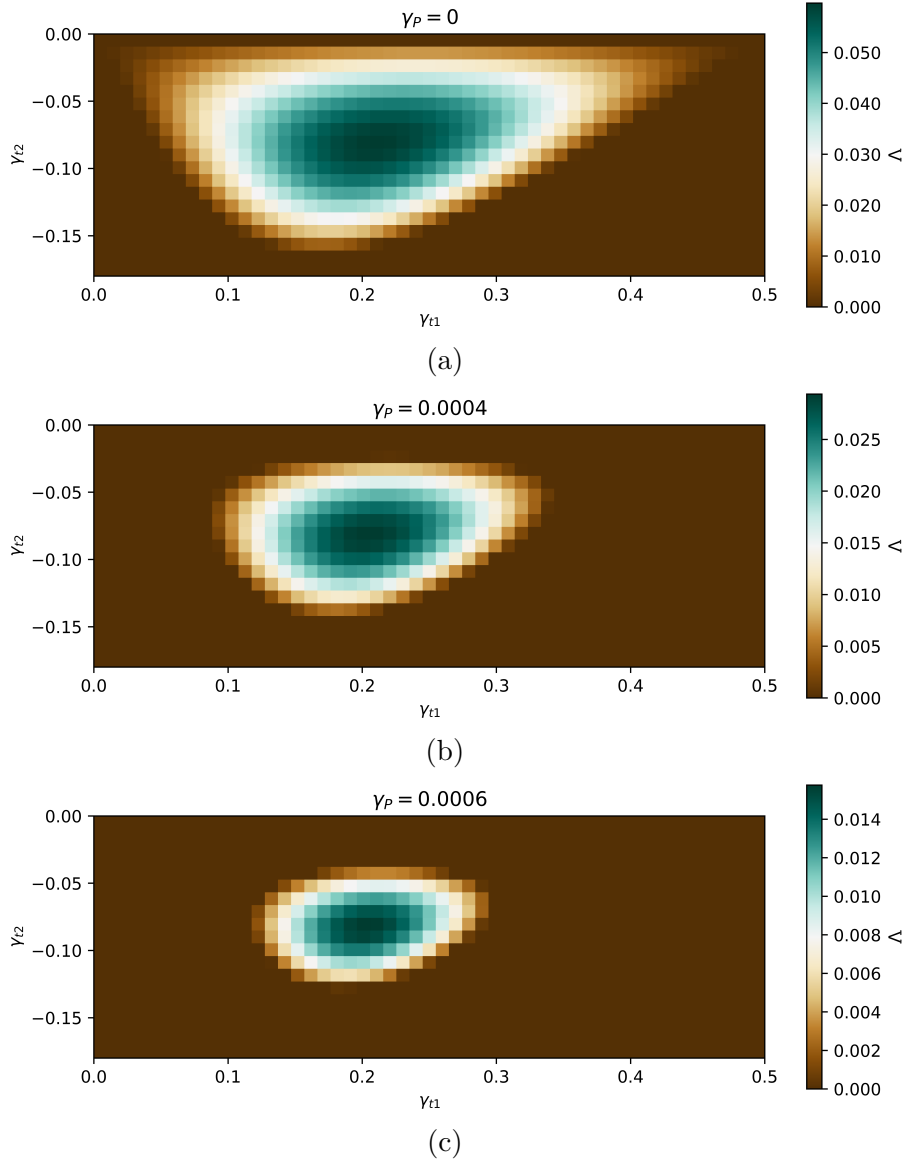


Figure 5.3: Heatmaps of the deviation  $\Lambda$  from complete positivity in the parameter space of the effective map under motional dephasing. Subfigures (a), (b), and (c) correspond to dissipation rates  $\gamma_P = 0$ , 0.0004, and 0.0006, respectively. The simulations are performed in the general field coupling regime with parameters  $\eta = 0.1$ ,  $\delta = 0.05\nu$ ,  $\Omega = 0.177\nu$ , and  $n_{\text{th}} = 0.05$ .

The main results are shown in Fig. 5.3. Owing to the central symmetry of the parameter space, we restrict attention to the fourth quadrant, i.e.  $\gamma_{t1} \in [0, 0.5]$  and  $\gamma_{t2} \in [-0.18, 0]$ . As shown in the figure, increasing the dissipation rate  $\gamma_P$  from 0 to 0.0006 causes the non-CP region to shrink and simultaneously reduces the overall deviation  $\Lambda$ . Throughout this process, the degree of non-CP behavior decreases at every point in parameter space.

The apparent changes in the shape of the region arise from numerical precision constraints. In particular, when the minimum eigenvalue  $\lambda_{\min}$  exceeds  $-10^{-5}$ , it is set to zero. Consequently, points that would otherwise yield small but finite deviations in Fig. 5.3(a) are automatically mapped to  $\Lambda = 0$  as  $\gamma_P$  increases. This limitation stems from the default numerical tolerance of `mesolve`, which is  $\sim 10^{-6}$ . While it is in principle possible to reduce the solver tolerance further, doing so would dramatically increase the integration time due to prohibitively small step sizes.

Further tests reveal that once the motional dephasing rate  $\gamma_P$  exceeds approximately 0.0009, the non-CP region in the parameter space vanishes entirely. In other words, sufficiently strong dissipation suppresses and eventually eliminates the non-complete positivity of the effective map.

At first sight this outcome is counterintuitive. A standard intuition is that non-CP maps arise precisely because the system and environment share correlations at the beginning of a reduced dynamical step. From this perspective, one would expect the persistence of qubit-motion correlations after the first MS gate to guarantee the possibility of non-CP reduced dynamics. Yet here, even though motional dephasing does not destroy the qubit-motion correlations themselves, it renders them ineffective for mediating information backflow, so that the effective map becomes CP once dissipation is sufficiently strong.

This suggests that correlations themselves are not the essential resource. Rather, the decisive factor lies in the specific patterns of information flow. Recall Fig. 3.2, motional dissipation disrupts precisely this channel: it degrades the phase coherence of the motional mode that the second MS gate would otherwise exploit to return information to the qubit. Thus, the disappearance of non-CP behavior is not due to the absence of correlations, but to the loss of their operational accessibility for information backflow.

In summary, these results point to a refinement of the correlation-based picture: it is not correlations alone, but correlations that are operationally accessible for information backflow, that enable non-CP reduced dynamics. Dissipation suppresses this accessibility and thereby restores complete positivity. This perspective provides a natural bridge between the mathematical characterization of non-CP maps and the information-theoretic description of non-Markovian dynamics.

From a practical standpoint, however, the threshold  $\gamma_P \approx 0.0009$  represents a rather stringent experimental condition: in real trapped-ion platforms, maintaining dissipation below this critical value is highly challenging. This makes it difficult to simulate non-Markovian dynamics simply by repeating miscalibrated MS gates. Nevertheless, the exploration of non-CP regions in the parameter space of multiple time-miscalibrated MS gates remains worthwhile—not only for deepening our understanding of the fundamental mechanisms, but also for identifying routes toward potential experimental realizations.

# 6

## Conclusions

This thesis has theoretically investigated three interconnected aspects of qubit-motion entanglement in the MS gate, spanning from fundamental mechanisms to practical implications for QC. First, I examined how qubit-motion entanglement mediates the flow of quantum information under both coherent and dissipative MS evolution. Second, I analyzed the noise structure arising from time miscalibration, deriving its mathematical form. Third, I explored circuit models of repetitive time-miscalibrated MS gates, identifying the parameter conditions under which non-CP maps emerge and how dissipation suppresses them. Collectively, these results deepen the understanding of how motional degrees of freedom govern the loss and recovery of quantum information, clarify the structure of time miscalibration, and elucidate the theoretical feasibility of exploiting residual entanglement as a resource for simulating non-Markovian dynamics.

In the first part, I employed the trace distance as a reliable quantity to visualize and quantify the information flow mediated by qubit-motion entanglement during MS evolution, both in the ideal coherent regime and under the influence of motional dissipation.

In the coherent case, the trace distance  $D$  exhibits pronounced periodic oscillations, each cycle corresponding to a closed trajectory of the motional state in phase space. Within a single period,  $D$  first decreases and then increases, reflecting the bidirectional exchange of information: qubits lose information to the motion, reducing their distinguishability, before the motion subsequently returns information to the qubits, restoring distinguishability. This demonstrates that the reduced qubit dynamics is intrinsically non-Markovian. Furthermore, comparisons across coupling regimes reveal that stronger field coupling accelerates the oscillations and amplifies the non-Markovian backflow, while the analysis across different initial state pairs highlights the necessity of sampling a sufficiently broad set of input states to faithfully capture non-Markovian behavior. When motional dissipation is introduced, its effect is revealed in two ways: a reduction of oscillation amplitude in  $D$ , reflecting the progressive suppression of qubit-motion information exchange, and a downward drift of  $D$ , which introduces a persistent negative bias in  $\sigma(t) = D(t)$ . Consequently, after a finite critical time  $t_c$ , the trace distance becomes strictly monotonic and the

---

qubit dynamics effectively transitions to a Markovian regime. Physically, this means that motional dissipation not only drains information from the total qubit-motion system, but also renders the motional mode incapable of returning stored information to the qubits, leading to irreversible information loss via the very entanglement that once enabled non-Markovian backflow.

Taken together, these findings directly address the central question of this part of the project: motional degrees of freedom govern the fate of quantum information in the qubits by mediating its bidirectional exchange in the coherent case, and by enabling its irreversible leakage under dissipation. The trace distance analysis thus provides both a conceptual and quantitative framework for understanding how qubit-motion entanglement serves as the channel through which quantum information is lost.

In the second part, time miscalibration in the MS gate was analyzed as a representative noise mechanism resulting in qubit-motion residual entanglement. By deriving the analytical form of the MS propagator under such imperfections, I showed that it can be factorized into a noiseless MS gate  $U_{\text{MS}}$  and two distinct error gates:  $V_m$ , originating from undesired qubit-motion entanglement, and  $V_q$ , corresponding to an effective additional spin-spin interaction independent of the motional state. This decomposition provides both a transparent physical picture and a practical mathematical tool:  $V_m$  captures the residual entanglement due to an open phase-space trajectory, while  $V_q$  represents a coherent over-rotation of the qubits. Together, these results reveal how time miscalibration induces effects closely analogous to those caused by symmetric detuning errors, where imperfect parameter settings likewise prevent the motional trajectory from closing.

Beyond the unitary decomposition, I further represented the effect of time miscalibration as a quantum channel in the Kraus-operator form. This analysis uncovered a fixed noise structure that is mathematically identical to that of motional dephasing, with only the coefficients depending on system parameters and error magnitude. This structural equivalence is highly instructive: despite their distinct physical origins, two very different noise sources act through the same effective error channel.

Overall, this study provides a refined characterization of MS-gate noise arising from time miscalibration. By clarifying both its unitary structure and its channel representation, these results not only deepen the understanding of how parameter calibration errors lead to qubit-motion residual entanglement, but also point toward unified strategies for analyzing and mitigating different error sources within trapped-ion quantum gates.

In the circuit model consisting of two repetitive time-miscalibrated MS gates, I found that non-CP behavior emerges only when the two time-miscalibration parameters have opposite signs. This shows that the appearance of non-complete positivity is subject to nontrivial constraints, rather than being a generic consequence of qubit-motion residual entanglement. Conversely, the reduced qubit dynamics remains CP whenever the second gate is ideal, or when both gates are miscalibrated in the same direction, even if the intermediate state carries qubit-motion correlations. These results establish a clear principle: correlations stored in the motion do not by themselves guarantee non-CP dynamics and they can affect complete positivity only if

the subsequent gate channels this information back into the qubits under specific conditions.

When motional dephasing is included, the heatmaps reveal that increasing the dissipation rate progressively shrinks the non-CP region and reduces the deviation from complete positivity across the entire parameter space. Once the rate exceeds  $\gamma_P \approx 0.0009$ , the non-CP region vanishes entirely. Interestingly, this occurs even though qubit-motion correlations are not destroyed by motional dephasing. Instead, dissipation renders them ineffective for mediating information backflow. This indicates that it is not correlations alone, but their operational accessibility for information flow, that enables non-CP reduced dynamics. Dissipation suppresses this accessibility and thereby restores complete positivity.

From a practical perspective, however, the threshold  $\gamma_P \approx 0.0009$  represents a demanding experimental condition. In real trapped-ion platforms, keeping motional dissipation below this value is highly challenging, which makes it difficult to simulate non-Markovian dynamics by simply repeating miscalibrated MS gates. Nonetheless, mapping out the non-CP regions in the parameter space of multiple miscalibrated MS gates remains valuable—not only for advancing the theoretical understanding of non-CP dynamics and information flow, but also for identifying possible pathways toward experimental realizations in more favorable regimes.

The findings of this thesis open several avenues for future investigation. First, the link between non-CP maps and information flow, though strongly suggested by the present results, remains to be formalized. Developing a unified framework that connects complete positivity, information backflow, and preparation dependence would deepen the conceptual foundations of open quantum dynamics. Second, extending the analysis to more complex circuit architectures, involving multiple time-miscalibrated MS gates or hybrid error sources, may uncover richer structures of non-CP dynamics and their controllability. Third, it would be valuable to further investigate why two physically distinct noise sources—motional dephasing and time miscalibration—yield error channels with the same Kraus structure. Understanding this structural equivalence may provide new strategies for unifying the treatment of diverse MS-gate noise processes and guiding error mitigation in practical implementations.

Finally, bridging theory with experiment represents a crucial next step. A concrete approach would be to employ the proposed circuit of two time-miscalibrated MS gates, and to contrast theoretical predictions obtained after tracing out the motional mode at the intermediate step with experimental dynamics obtained without partial trace. Such an analysis, carried out via trace distance, could provide a systematic framework for quantifying and interpreting deviations between theoretical models and experimental realizations.

# References

- [1] John Preskill. “Quantum Computing in the NISQ era and beyond.” In: *Quantum* 2 (Aug. 6, 2018), p. 79. ISSN: 2521-327X. DOI: [10.22331/q-2018-08-06-79](https://doi.org/10.22331/q-2018-08-06-79). URL: <https://quantum-journal.org/papers/q-2018-08-06-79/> (visited on 06/29/2025).
- [2] Colin D. Bruzewicz et al. “Trapped-ion quantum computing: Progress and challenges.” In: *Applied Physics Reviews* 6.2 (June 1, 2019), p. 021314. ISSN: 1931-9401. DOI: [10.1063/1.5088164](https://doi.org/10.1063/1.5088164). URL: <https://pubs.aip.org/apr/article/6/2/021314/570103/Trapped-ion-quantum-computing-Progress-and> (visited on 02/27/2025).
- [3] Wen-Han Png et al. “Quantum Computing With Trapped Ions: An overview.” In: *IEEE Nanotechnology Mag.* 16.4 (Aug. 2022), pp. 30–36. ISSN: 1932-4510, 1942-7808. DOI: [10.1109/MNANO.2022.3175384](https://doi.org/10.1109/MNANO.2022.3175384). URL: <https://ieeexplore.ieee.org/document/9797817/> (visited on 09/03/2025).
- [4] W. Neuhauser et al. “Localized visible Ba + mono-ion oscillator.” In: *Phys. Rev. A* 22.3 (Sept. 1, 1980), pp. 1137–1140. ISSN: 0556-2791. DOI: [10.1103/PhysRevA.22.1137](https://doi.org/10.1103/PhysRevA.22.1137). URL: <https://link.aps.org/doi/10.1103/PhysRevA.22.1137> (visited on 02/27/2025).
- [5] Anders Sørensen and Klaus Mølmer. “Quantum Computation with Ions in Thermal Motion.” In: *Phys. Rev. Lett.* 82.9 (Mar. 1, 1999), pp. 1971–1974. ISSN: 0031-9007, 1079-7114. DOI: [10.1103/PhysRevLett.82.1971](https://doi.org/10.1103/PhysRevLett.82.1971). URL: <https://link.aps.org/doi/10.1103/PhysRevLett.82.1971> (visited on 02/13/2025).
- [6] Anders Sørensen and Klaus Mølmer. “Entanglement and quantum computation with ions in thermal motion.” In: *Phys. Rev. A* 62.2 (July 18, 2000), p. 022311. ISSN: 1050-2947, 1094-1622. DOI: [10.1103/PhysRevA.62.022311](https://doi.org/10.1103/PhysRevA.62.022311). URL: <https://link.aps.org/doi/10.1103/PhysRevA.62.022311> (visited on 02/13/2025).
- [7] C. J. Ballance et al. “High-Fidelity Quantum Logic Gates Using Trapped-Ion Hyperfine Qubits.” en. In: *Phys. Rev. Lett.* 117.6 (Aug. 2016), p. 060504. ISSN: 0031-9007, 1079-7114. DOI: [10.1103/PhysRevLett.117.060504](https://doi.org/10.1103/PhysRevLett.117.060504). URL: <https://link.aps.org/doi/10.1103/PhysRevLett.117.060504> (visited on 02/13/2025).
- [8] Ye Wang et al. “High-Fidelity Two-Qubit Gates Using a Microelectromechanical-System-Based Beam Steering System for Individual Qubit Addressing.” In: *Phys. Rev. Lett.* 125.15 (Oct. 6, 2020), p. 150505. ISSN: 0031-9007, 1079-7114. DOI: [10.1103/PhysRevLett.125.150505](https://doi.org/10.1103/PhysRevLett.125.150505). URL: <https://link.aps.org/doi/10.1103/PhysRevLett.125.150505> (visited on 06/29/2025).

- [9] Chao Fang et al. “Crosstalk Suppression in Individually Addressed Two-Qubit Gates in a Trapped-Ion Quantum Computer.” In: *Phys. Rev. Lett.* 129.24 (Dec. 7, 2022), p. 240504. ISSN: 0031-9007, 1079-7114. DOI: [10.1103/PhysRevLett.129.240504](https://doi.org/10.1103/PhysRevLett.129.240504). URL: <https://link.aps.org/doi/10.1103/PhysRevLett.129.240504> (visited on 06/29/2025).
- [10] Y.-H. Hou et al. “Individually addressed entangling gates in a two-dimensional ion crystal.” en. In: *Nat Commun* 15.1 (Nov. 2024), p. 9710. ISSN: 2041-1723. DOI: [10.1038/s41467-024-53405-z](https://doi.org/10.1038/s41467-024-53405-z). URL: <https://www.nature.com/articles/s41467-024-53405-z> (visited on 09/08/2025).
- [11] Farhang Haddadfarshi and Florian Mintert. “High fidelity quantum gates of trapped ions in the presence of motional heating.” In: *New J. Phys.* 18.12 (Dec. 2, 2016), p. 123007. ISSN: 1367-2630. DOI: [10.1088/1367-2630/18/12/123007](https://doi.org/10.1088/1367-2630/18/12/123007). URL: <https://iopscience.iop.org/article/10.1088/1367-2630/18/12/123007> (visited on 02/13/2025).
- [12] A. E. Webb et al. “Resilient Entangling Gates for Trapped Ions.” In: *Phys. Rev. Lett.* 121.18 (Nov. 1, 2018), p. 180501. ISSN: 0031-9007, 1079-7114. DOI: [10.1103/PhysRevLett.121.180501](https://doi.org/10.1103/PhysRevLett.121.180501). URL: <https://link.aps.org/doi/10.1103/PhysRevLett.121.180501> (visited on 02/13/2025).
- [13] B. P. Ruzic et al. “Entangling-gate error from coherently displaced motional modes of trapped ions.” en. In: *Phys. Rev. A* 105.5 (May 2022), p. 052409. ISSN: 2469-9926, 2469-9934. DOI: [10.1103/PhysRevA.105.052409](https://doi.org/10.1103/PhysRevA.105.052409). URL: <https://link.aps.org/doi/10.1103/PhysRevA.105.052409> (visited on 09/08/2025).
- [14] Fernando Martínez-García et al. “Analytical and experimental study of center-line miscalibrations in Mølmer-Sørensen gates.” en. In: *Phys. Rev. A* 105.3 (Mar. 2022), p. 032437. ISSN: 2469-9926, 2469-9934. DOI: [10.1103/PhysRevA.105.032437](https://doi.org/10.1103/PhysRevA.105.032437). URL: <https://link.aps.org/doi/10.1103/PhysRevA.105.032437> (visited on 09/08/2025).
- [15] Ke Sun et al. “Quantum simulation of spin-boson models with structured bath.” en. In: *Nat Commun* 16.1 (Apr. 2025), p. 4042. ISSN: 2041-1723. DOI: [10.1038/s41467-025-59296-y](https://doi.org/10.1038/s41467-025-59296-y). URL: <https://www.nature.com/articles/s41467-025-59296-y> (visited on 09/04/2025).
- [16] Peter W. Shor. “Scheme for reducing decoherence in quantum computer memory.” In: *Phys. Rev. A* 52.4 (Oct. 1, 1995), R2493–R2496. ISSN: 1050-2947, 1094-1622. DOI: [10.1103/PhysRevA.52.R2493](https://doi.org/10.1103/PhysRevA.52.R2493). URL: <https://link.aps.org/doi/10.1103/PhysRevA.52.R2493> (visited on 06/29/2025).
- [17] A. R. Calderbank and Peter W. Shor. “Good quantum error-correcting codes exist.” In: *Phys. Rev. A* 54.2 (Aug. 1, 1996), pp. 1098–1105. ISSN: 1050-2947, 1094-1622. DOI: [10.1103/PhysRevA.54.1098](https://doi.org/10.1103/PhysRevA.54.1098). URL: <https://link.aps.org/doi/10.1103/PhysRevA.54.1098> (visited on 06/29/2025).
- [18] “Multiple-particle interference and quantum error correction.” In: *Proc. R. Soc. Lond. A* 452.1954 (Nov. 8, 1996), pp. 2551–2577. ISSN: 1364-5021, 1471-2946. DOI: [10.1098/rspa.1996.0136](https://doi.org/10.1098/rspa.1996.0136). URL: <https://royalsocietypublishing.org/doi/10.1098/rspa.1996.0136> (visited on 06/29/2025).

- [19] Robert Raussendorf and Jim Harrington. “Fault-Tolerant Quantum Computation with High Threshold in Two Dimensions.” In: *Phys. Rev. Lett.* 98.19 (May 11, 2007), p. 190504. ISSN: 0031-9007, 1079-7114. DOI: [10.1103/PhysRevLett.98.190504](https://doi.org/10.1103/PhysRevLett.98.190504). URL: <https://link.aps.org/doi/10.1103/PhysRevLett.98.190504> (visited on 02/27/2025).
- [20] Robert Raussendorf. “Key ideas in quantum error correction.” In: *Phil. Trans. R. Soc. A.* 370.1975 (Sept. 28, 2012), pp. 4541–4565. ISSN: 1364-503X, 1471-2962. DOI: [10.1098/rsta.2011.0494](https://doi.org/10.1098/rsta.2011.0494). URL: <https://royalsocietypublishing.org/doi/10.1098/rsta.2011.0494> (visited on 04/03/2025).
- [21] Zhenyu Cai et al. “Quantum error mitigation.” In: *Rev. Mod. Phys.* 95.4 (Dec. 13, 2023), p. 045005. ISSN: 0034-6861, 1539-0756. DOI: [10.1103/RevModPhys.95.045005](https://doi.org/10.1103/RevModPhys.95.045005). URL: <https://link.aps.org/doi/10.1103/RevModPhys.95.045005> (visited on 06/28/2025).
- [22] Yue Ma and M. S. Kim. “Limitations of probabilistic error cancellation for open dynamics beyond sampling overhead.” In: *Phys. Rev. A* 109.1 (Jan. 25, 2024), p. 012431. ISSN: 2469-9926, 2469-9934. DOI: [10.1103/PhysRevA.109.012431](https://doi.org/10.1103/PhysRevA.109.012431). URL: <https://link.aps.org/doi/10.1103/PhysRevA.109.012431> (visited on 06/28/2025).
- [23] José D. Guimarães et al. “Noise-Assisted Digital Quantum Simulation of Open Systems Using Partial Probabilistic Error Cancellation.” In: *PRX Quantum* 4.4 (Nov. 21, 2023), p. 040329. ISSN: 2691-3399. DOI: [10.1103/PRXQuantum.4.040329](https://doi.org/10.1103/PRXQuantum.4.040329). URL: <https://link.aps.org/doi/10.1103/PRXQuantum.4.040329> (visited on 06/28/2025).
- [24] Juha Leppäkangas et al. “Quantum algorithm for solving open-system dynamics on quantum computers using noise.” In: *Phys. Rev. A* 108.6 (Dec. 22, 2023), p. 062424. ISSN: 2469-9926, 2469-9934. DOI: [10.1103/PhysRevA.108.062424](https://doi.org/10.1103/PhysRevA.108.062424). URL: <https://link.aps.org/doi/10.1103/PhysRevA.108.062424> (visited on 06/28/2025).
- [25] Yue Ma et al. *Reshaping quantum device noise via repetition code circuits*. May 19, 2025. DOI: [10.48550/arXiv.2411.00751](https://doi.org/10.48550/arXiv.2411.00751). arXiv: [2411.00751\[quant-ph\]](https://arxiv.org/abs/2411.00751). URL: [http://arxiv.org/abs/2411.00751](https://arxiv.org/abs/2411.00751) (visited on 06/03/2025).
- [26] Philip Pechukas. “Reduced Dynamics Need Not Be Completely Positive.” en. In: *Phys. Rev. Lett.* 73.8 (Aug. 1994), pp. 1060–1062. ISSN: 0031-9007. DOI: [10.1103/PhysRevLett.73.1060](https://doi.org/10.1103/PhysRevLett.73.1060). URL: <https://link.aps.org/doi/10.1103/PhysRevLett.73.1060> (visited on 08/13/2025).
- [27] Heinz-Peter Breuer, Elsi-Mari Laine, and Jyrki Piilo. “Measure for the Degree of Non-Markovian Behavior of Quantum Processes in Open Systems.” en. In: *Phys. Rev. Lett.* 103.21 (Nov. 2009). Publisher: American Physical Society (APS). ISSN: 0031-9007, 1079-7114. DOI: [10.1103/physrevlett.103.210401](https://doi.org/10.1103/physrevlett.103.210401). URL: <https://link.aps.org/doi/10.1103/PhysRevLett.103.210401> (visited on 07/21/2025).

- [28] Mirko Rossini et al. “Single-Qubit Error Mitigation by Simulating Non-Markovian Dynamics.” en. In: *Phys. Rev. Lett.* 131.11 (Sept. 2023). Publisher: American Physical Society (APS). ISSN: 0031-9007, 1079-7114. DOI: [10.1103/physrevlett.131.110603](https://doi.org/10.1103/physrevlett.131.110603). URL: <https://link.aps.org/doi/10.1103/PhysRevLett.131.110603> (visited on 07/18/2025).
- [29] J.R. Johansson, P.D. Nation, and Franco Nori. “QuTiP 2: A Python framework for the dynamics of open quantum systems.” In: *Computer Physics Communications* 184.4 (2013), pp. 1234–1240. ISSN: 0010-4655. DOI: <https://doi.org/10.1016/j.cpc.2012.11.019>. URL: <https://www.sciencedirect.com/science/article/pii/S0010465512003955>.
- [30] Neill Lambert et al. “QuTiP 5: The Quantum Toolbox in Python.” In: (2024). arXiv: [2412.04705 \[quant-ph\]](https://arxiv.org/abs/2412.04705). URL: <https://arxiv.org/abs/2412.04705>.
- [31] Michael A. Nielsen and Isaac L. Chuang. *Quantum computation and quantum information*. 10th anniversary ed. Cambridge ; New York: Cambridge University Press, 2010. ISBN: 978-1-107-00217-3.
- [32] J. I. Cirac and P. Zoller. “Quantum Computations with Cold Trapped Ions.” In: *Phys. Rev. Lett.* 74.20 (May 15, 1995), pp. 4091–4094. ISSN: 0031-9007, 1079-7114. DOI: [10.1103/PhysRevLett.74.4091](https://doi.org/10.1103/PhysRevLett.74.4091). URL: <https://link.aps.org/doi/10.1103/PhysRevLett.74.4091> (visited on 03/05/2025).
- [33] S. Blanes et al. “The Magnus expansion and some of its applications.” en. In: *Physics Reports* 470.5-6 (Jan. 2009), pp. 151–238. ISSN: 03701573. DOI: [10.1016/j.physrep.2008.11.001](https://doi.org/10.1016/j.physrep.2008.11.001). URL: <https://linkinghub.elsevier.com/retrieve/pii/S0370157308004092> (visited on 09/08/2025).
- [34] Modesto Orozco-Ruiz, Wasim Rehman, and Florian Mintert. *Generally noise-resilient quantum gates for trapped-ions*. arXiv:2404.12961 [quant-ph]. Apr. 2024. DOI: [10.48550/arXiv.2404.12961](https://doi.org/10.48550/arXiv.2404.12961). URL: [http://arxiv.org/abs/2404.12961](https://arxiv.org/abs/2404.12961) (visited on 02/13/2025).
- [35] Yao Lu et al. “Global entangling gates on arbitrary ion qubits.” In: *Nature* 572.7769 (Aug. 2019), pp. 363–367. ISSN: 0028-0836, 1476-4687. DOI: [10.1038/s41586-019-1428-4](https://doi.org/10.1038/s41586-019-1428-4). URL: <https://www.nature.com/articles/s41586-019-1428-4> (visited on 03/06/2025).
- [36] Nguyen H. Le et al. *Amplitude-noise-resilient entangling gates for trapped ions*. arXiv:2407.03047 [quant-ph]. July 2024. DOI: [10.48550/arXiv.2407.03047](https://doi.org/10.48550/arXiv.2407.03047). URL: [http://arxiv.org/abs/2407.03047](https://arxiv.org/abs/2407.03047) (visited on 02/13/2025).
- [37] G. Lindblad. “On the generators of quantum dynamical semigroups.” In: *Commun. Math. Phys.* 48.2 (June 1976), pp. 119–130. ISSN: 0010-3616, 1432-0916. DOI: [10.1007/BF01608499](https://doi.org/10.1007/BF01608499). URL: [http://link.springer.com/10.1007/BF01608499](https://link.springer.com/10.1007/BF01608499) (visited on 02/13/2025).
- [38] Man-Duen Choi. “Completely positive linear maps on complex matrices.” en. In: *Linear Algebra and its Applications* 10.3 (June 1975), pp. 285–290. ISSN: 00243795. DOI: [10.1016/0024-3795\(75\)90075-0](https://doi.org/10.1016/0024-3795(75)90075-0). URL: <https://linkinghub.elsevier.com/retrieve/pii/0024379575900750> (visited on 09/08/2025).

- [39] K Kraus. “General state changes in quantum theory.” en. In: *Annals of Physics* 64.2 (June 1971), pp. 311–335. ISSN: 00034916. DOI: [10.1016/0003-4916\(71\)90108-4](https://doi.org/10.1016/0003-4916(71)90108-4). URL: <https://linkinghub.elsevier.com/retrieve/pii/0003491671901084> (visited on 09/08/2025).
- [40] Christopher J. Wood, Jacob D. Biamonte, and David G. Cory. “Tensor networks and graphical calculus for open quantum systems.” In: (2011). Publisher: arXiv Version Number: 3. DOI: [10.48550/ARXIV.1111.6950](https://doi.org/10.48550/ARXIV.1111.6950). URL: <https://arxiv.org/abs/1111.6950> (visited on 09/08/2025).
- [41] Lukas Hantzko, Lennart Binkowski, and Sabhyata Gupta. *Fast generation of Pauli transfer matrices utilizing tensor product structure*. Version Number: 2. 2024. DOI: [10.48550/ARXIV.2411.00526](https://doi.org/10.48550/ARXIV.2411.00526). URL: <https://arxiv.org/abs/2411.00526> (visited on 09/08/2025).